AN INVESTIGATION INTO THE PLASTIC BUCKLING PARADOX FOR CIRCULAR CYLINDRICAL SHELLS UNDER NON-PROPORTIONAL LOADING

Rabee Shamass[1,*], Giulio Alfano[1], Federico Guarracino[2]

1 - Collage of Engineering, Design and Physical Sciences, Brunel University, UB8 3PH Uxbridge, UK

2 – University of Naples 'Federico II', Via Claudio 21, 80125 Napoli, Italy

Abstract

Many authors in the literature agreed that the flow theory of plasticity either fails to predict buckling or overestimates plastic buckling stresses and strains of plates and shells while the deformation theory succeeds in forecasting buckling and provides estimates that are more in line with the experimental results. Following a previous study by the same authors focused on compressed cylinders, the present work aims to investigate the reasons for the discrepancy between the flow and deformation theory predictions in the case of cylinders subjected to combined axial tensile load and increasing external lateral pressure. To this end, geometrically nonlinear finite-element calculations of selected cylindrical shells using both the flow theory and the deformation theory of plasticity have been conducted, and the results are compared with some accurate physical test results and with numerical results obtained by other authors using the code BOSOR5. It is found, contrary to common belief, that very good agreement between numerical and test results can be obtained in the case of the flow theory of plasticity. The reasons underlying the apparent plastic buckling paradox are discussed in detail.

Keywords: shell buckling; shell instability; plastic buckling; deformation plasticity; flow plasticity; plastic paradox; non-linear FEA; non-proportional loading.

*   Corresponding author. Tel.: +44 7411979619.
    E-mail addresses: Rabee.Shamass@brunel.ac.uk, rabeeshammas@yahoo.com
(R. Shamass).

1. Introduction

Plastic buckling of circular cylindrical shells has been the subject of intense research for many decades due to its importance in many engineering applications. In particular, many experimental, analytical and numerical studies have been conducted to investigate buckling of cylinders subject to axial compression, external pressure, torsion or combination of such load cases.

In general, accurate numerical or analytical estimation of the critical load of plastic buckling of real cylinders requires accounting for moderate large deflection and, nonlinear, irreversible (i.e. path-dependent) material behaviour (Bushnell, 1986).

As for the material constitutive law to be used, the plasticity models that have been proposed for metals fall within one of two different theories: the 'deformation theory' of plasticity and the 'flow theory' of plasticity. In both of these theories the plastic-strain increments are isochoric, i.e. characterised by zero volume change, and their evolution is governed by the second invariant J_2 of the deviatoric part of the stress. The flow theory of plasticity defines a path-dependent law, in which the current stress depends not only on the value of the current total strain but also on how the actual strain value has been reached. On the other hand, the deformation theory of plasticity is based on the assumption that for continued loading the state of stress is uniquely determined by the current state of strain and, therefore, it is a special class of path-independent non-linear elastic constitutive laws.

Experimental investigations show that plastic strains depend both on the the stress value and the loading history. Thus, there is general agreement among engineers and researchers that the deformation theory of plasticity lacks of physical rigour with respect to the flow theory. However many authors, such as Onat and Drucker (1953), Mao and Lu (1999), Durban and Ore (1992) and Bardi and Kyriakides (2006), among the others, pointed out that the deformation theory tends to predict buckling loads that are smaller than those obtained by the flow theory and much closer to the experimental results. In fact, the flow theory seems to over-estimate buckling loads, often quite significantly.

There have been many attempts to explain this so called ''plastic buckling paradox'' and formulate accurate methods based on the flow theory of plasticity, that typically differ from each other on account of the choice and formulation of the constitutive

equations and of the associated factors. For instance, Batdorf and Budiansky (1949) suggested to use the slip theory in plastic buckling analysis. Sewell (1973) proposed the use of Tresca yield surface in the flow theory of plasticity and Lay (1965) proposed that the effective shear modulus should be employed when using the flow theory, whereas Ambartsumjan (1963) recommended considering the transverse shear deformation. Attention was also paid to the consideration of initial imperfections, as proposed by Onat and Drucker (1953).

More recently, Shamass et al. (2014) numerically investigated buckling of axially compressed cylindrical shells in the plastic range. They showed that non-linear finite-element buckling analyses based on the flow theory provide buckling stresses in better agreement with the experimental results than those based on the deformation theory, a fact that is in contrast with the conclusions by Mao and Lu (1999), Durban and Ore (1992) and Bardi and Kyriakides (2006). Shamass et al. (2014) concluded that the main root of the discrepancy between the two plasticity theories can be found in the assumptions made in many analytical treatments with regard to the shape of the buckling modes, a simplification which gives origin to an excessively constrained kinematics, in turn counterbalanced by the material description of the deformation theory of plasticity. This fact has also been confirmed to a certain extent by analytical investigations (Shamass et al., 2015).

In the case of axially loaded cylinders, at least during the elastic phase, the walls are subjected to proportional loading, and in many points during plastic yielding the deviation from the loading path is relatively limited. Nevertheless, the flow and deformation theory seem to provide quite different results.

It is therefore not surprising that similar or even more significant discrepancies have been reported between the results from the flow and deformation theory in the case of non-proportional loading even in the elastic phase.

Blachut et al. (1996) conducted experimental and numerical analyses on 30 mild-steel machined cylinders of different dimensions, subject to axial tension and increasing external pressure. Using the code BOSOR5 (Bushnell, 1986) for their numerical analyses they showed that the agreement between the two plasticity theories was strongly dependent on the length of the cylindrical shell. For short cylinders ($D/L = 1$), the plastic buckling results predicted by the flow and deformation theory coincided only when the tensile axial load vanished. By increasing the axial tensile load, the buckling

pressures predicted by the flow theory started to diverge quickly from those predicted by the deformation theory. Additionally, the flow theory failed to predict buckling for high axial tensile load while tests confirmed the buckling occurrence. For specimens with length-to-diameter ratio L/D ranging from 1.5 to 2.0 the results predicted by both theories were identical for a certain range of combined loading. However, for high values of the applied tensile load, the predictions of the flow theory began to deviate from those of the deformation theory and became unrealistic in correspondence to large plastic strains.

Giezen et al. (1991) conducted experiments and numerical analyses on two sets of tubes made of aluminium alloy 6061-T4 and subjected to combined axial tension and external pressure, once again making resort to the code BOSOR5 (Bushnell, 1986). The tubes were characterised by a L/D ratio equal to one and two loading paths were considered. In the first one the axial tensile load was held constant and the external pressure was increased. In the second one, the external pressure was held constant and the axial tensile load was increased. The numerical studies showed that the buckling pressure predicted by the flow theory increases with increasing applied tensile load while the experimental tests showed on the contrary a reduction in buckling resistance with increasing axial tension. Thus, the discrepancy between the test results and the numerical results predicted by the flow theory increased significantly with the intensification of the axial tension. On the other hand, the results by the deformation theory displayed the same trend of the test results. However, the deformation theory significantly under-predicted the buckling pressure observed experimentally for some load-paths. Therefore, Giezen (1988) concluded that both plasticity theories were unsuccessful in predicting buckling load. Interestingly enough, Giezen showed in his thesis (1988) that, when reversing the load path, the deformation theory was able to predict buckling while the flow theory failed to do so.

Tuğcu (1991) investigated analytically the buckling of cylinders under combined axial load and torque and combined external pressure and torque. He found that the predictions of the flow theory were more sensitive to the non-proportionality of loading than those of the deformation theory although the predictions of both theories were similar in some region of a particular interaction.

Overall, the above mentioned literature indicates that the flow theory has been generally found to be more sensitive with respect to non-proportional loading than the deformation theory.

In the case of cylinders subjected to axial tensile load and external pressure, Blachut et al. (1996) and Giezen et al. (1991) concluded that the flow theory tends to over predict quite significantly the plastic strains and the buckling loads in the case of high values of the axial tensile loads, while the deformation theory leads to results that seem more in line with the experimental observations.

Recently, attempts have been made to develop a revised deformation theory by including unloading (Peek, 2000) or to propose a total deformation theory applicable to non-proportional loading, defined as a sequence of linear loadings (Jahed et al., 1998).

The present work aims to shed further light on the plastic buckling paradox by means of carefully conducted finite-element (FE) analyses of cylindrical shells using both the flow theory and the deformation theory of plasticity. Results are compared with the experimental and the numerical results obtained by Blachut et al. (1996) and Giezen et al. (1991 using the code BOSOR5. The study also aims to examine the sensitivity of the predicted critical strains and buckling pressures with respect to the applied tensile load.

The analysis is focused on machined short cylindrical shells subjected to axial tension and increasing external pressure, with length-to-outer diameter ratio L/D ranging between 1 and 2.

The paper is organised as follows. Section 2 presents in details the finite-element (FE) modelling of selected cylindrical shells tested by the above mentioned authors by means of the code ABAQUS, version 6.11-1 (Simulia, 2011). Comparison of the FE results with the experimental and numerical results by Blachut et al. (1996) and Giezen et al. (1991) is presented in depth in Sections 3 and 4, respectively. Section 5 contains an comprehensive discussion of the results in order to provide an insight into the underpinning causes of the discrepancy between the present results and those by Blachut et al. (1996) and Giezen et al. (1991). Some conclusions are finally drawn in Section 6.

2. Test samples and finite-element modelling

2.1 Geometry and elements

The plastic buckling of selected imperfect cylinders tested by Blachut et al. (1996) and Giezen et al. (1991), subjected to uniform external pressure and axial tensile load, has been numerically simulated using non-linear FE analyses using both the flow theory and the deformation theory of plasticity, by means of the FE code ABAQUS, version 6.11-1 (Simulia, 2011).

2.1.1 Modelling of tests made by Blachut et al. (1996)

Blachut et al. (1996) conducted tests on 30 machined cylinders made of mild steel with outer diameter 34 mm and length to diameter ratio (L/D) of 1.0, 1.5 and 2.0. In the experimental setting, one flange of the specimen was rigidly attached to the end flange of the pressure chamber and the other flange was bolted to a coupling device which in turn was bolted to the load cell, see Figure 2.1. The load cell was centred with respect to the test chamber in order to prevent any eccentricity of the axial load exerted on the specimen. The authors reported that the maximum initial radial imperfection measured at the mid-length of the specimens was about 1% of the wall thickness.

In the present investigation, in order to keep the numerical analyses at a reasonable number, twelve cylinders were chosen, as illustrated in Table 2.1, in such a way that (a) a significant range of L/D is covered in the study and (b) for all the selected cases, except S2 and L4, the flow theory of plasticity failed to predict buckling numerically according to Blachut et al. (1996).
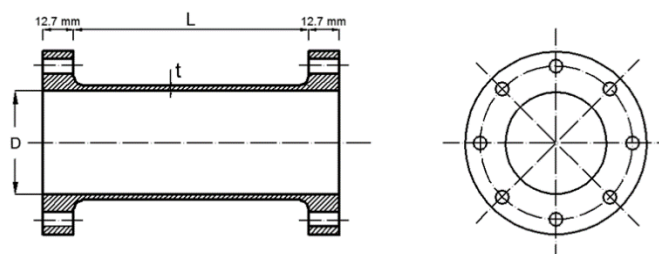

Figure2.1: Experimental setting.

Spec.	Geometry of the cylinders		
	$D\ (mm)$	$t\ (mm)$	L/D
S1	34.01	0.685	0.982
S2	33.98	0.688	0.983
S3	34.05	0.667	0.982
S4	34.07	0.667	0.982
S5	33.98	0.679	0.981
S6	34.06	0.704	0.979
S7	33.97	0.675	0.982
M2	34	0.616	1.47
M12	33.59	0.669	1.474
M7	33.97	0.63	1.473
L4	34	0.669	1.961
L8	33.96	0.693	1.964

Table 2.1: Geometry of tested cylinders.

In the FE modelling one reference point has been located at the centre of the top end of the cylinder and the axial displacements of all the nodes at the top edge of the cylinder have been constrained to the axial displacement of this reference point. The axial tensile load has been applied directly to the reference point. All the other degrees of freedom of the nodes at the top edge have been restrained. The bottom edge of the shell has been considered fully fixed, i.e. with no allowed translation or rotations at any node.
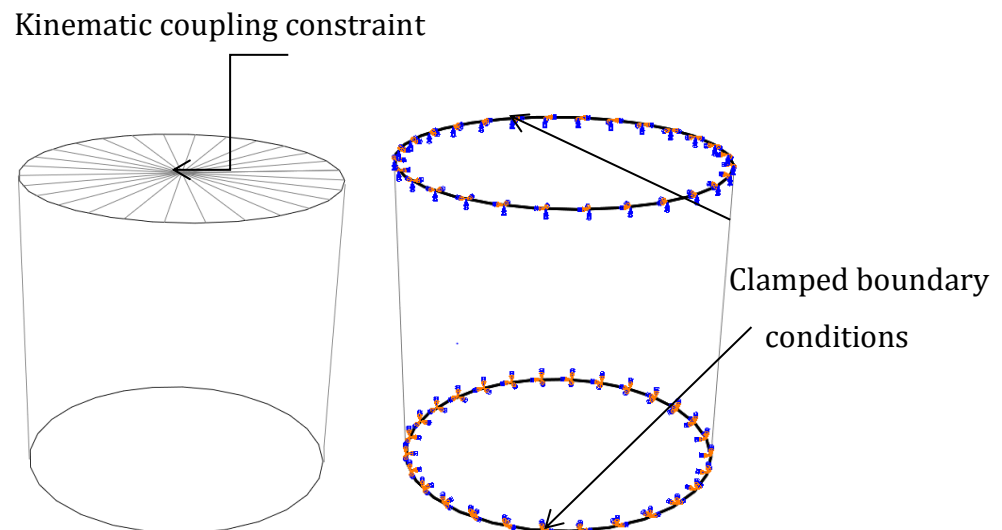
Figure 2.2: Boundary conditions.

In order to simulate the experimental settings, two types of loading have been considered: axial tensile load in the longitudinal direction and external pressure

applied normally to the surface of the shell elements (Table 2.2). First the tensile load has been applied and held constant. Successively, an increasing lateral pressure has been applied.

Specimen	S1	S2	S3	S4	S5	S6	S7
Axial tension (N)	17960	0	18000	3990	12010	15030	7970

Specimen	M2	M12	M7	L4	L8
Axial tension (N)	10670	18530	15060	8210	16490

Table2.2: Axial tension values for the selected cylinders.

The cylinders have been modelled by means of a general-purpose 4-noded fully-integrated shell element, "S4" (Simulia, 2011), which accounts for large deformations. Each node has six degrees of freedom and the element is based on a thick shell theory. It is widely used for industrial applications because it is suitable for both thin and thick shells. The strain approach is such as to prevent shear and membrane locking.

A structured mesh was used, made from a number of divisions along the circumference and longitudinal direction, as reported in Table 2.3 for each specimen.

Number of elements	Specimens						
	S1	S2	S3	S4	S5	S6	S7
- around the circumference	200	200	200	200	200	200	200
- along the length	63	63	63	63	63	63	63

Number of elements	Specimens				
	M2	M12	M7	L4	L8
- around the circumference	200	200	200	200	200
- along the length	94	94	94	125	125

Table 2.3: FE mesh discretisation adopted for the analyses of the cylinders tested by Blachut et al. (1996).

2.1.2 Modelling of tests made by Giezen et al. (1991)

In the test carried out by Giezen et al. (1991), the cylindrical specimens were made of aluminium alloy 6061-T4. Two sets of specimens were tested, namely Set A and Set B. The average wall-thickness values of the first and second set were 0.76 and 0.71 mm, respectively, and the length-to-diameter ratio (L/D) was equal to one. The maximum initial imperfections were found to be about 0.076mm (10% of the thickness) (Giezen et al., 1991).

For the present numerical analysis only the specimens subjected to constant axial tensile load and increasing external pressure have been taken into consideration, as shown in Tables 2.4 and 2.5.

Specimen	SP.1	SP.2	SP.3	SP.4	SP.5	SP.6	SP.7
Axial tension (N)	0	1254.41	2508.81	4076.82	5205.8	6021.15	6522.9
N. of buckling waves	5	5	5	5	4	4	4

Specimen	SP.8	SP.9	SP.10	SP.11	SP.12	SP.13
Axial tension (N)	6899.24	7902.77	9408.05	11666	12920.4	14613.84
N. of buckling waves	4	4	4	4	4	4

Table 2.4: Axial tensile load and observed number of buckling waves (in the circumferential direction) for Set A specimens

Specimen	SP.1	SP.2	SP.3	SP.4	SP.5	SP.6	SP.7
Axial tension (N)	0	2343.76	4793	7089.9	9375	11777.4	14062.6
N. of buckling waves	4	4	4	4	4	4	4

Table 2.5: Axial tensile load and observed number of buckling waves (in the circumferential direction) for Set B specimens.

Again, a 4-noded shell elements (S4) has been used with a structured mesh and a division of 210 and 67 elements along the circumference and the length, respectively. The same boundary conditions used to simulate Blachut's experiments were adopted.

2.2 Material parameters

The uniaxial stress-strain relationship of the material under monotonic loading has been characterised by means of the Ramberg-Osgood law, i.e.

$$E\varepsilon = \sigma + \alpha \left(\frac{\sigma}{\sigma_y}\right)^{n-1} \sigma \tag{2.1}$$

where σ and ε denote uniaxial stress and strain, E and v are theYoung's modulus and Poisson's ratio, σ_y is the nominal yield strength, α is the 'yield offset' and n is the hardening parameter.

The Ramberg-Osgood input parameters used in the numerical simulations are reported in Table 2.6.

	E [MPa]	σ_y[MPa]	v	n	α
Blachut's test	212000	328 or290	0.31	300	0.428
Giezen's test-Set A	65129.73	177.75	0.3	16	0.733
Giezen's test-Set B	60986.34	165.37	0.3	11.76	0.738

Table 2.6: Ramberg-Osgood constants used in the numerical analyses.

Blachut et al. (1996) conducted longitudinal tensile tests on a number of coupons to determine the mechanical properties of the cylindrical specimens. They reported that the yield plateau in the stress-strain relationship of the material appears to be extended to a strain value of almost 3%, see Figure 2.3. Moreover, they observed that the upper yield stress of the tested coupons, cut along the longitudinal direction of the cylinders, varied from 280 to 360 MPa, with an average value of 328 MPa, and the lower yield stress from 275 to 305 MPa, with an average value of 290 MPa (Blachut et al., 1996). In the present numerical analysis both the average upper yield stress, $\sigma_y^u = 328$Mpa, and the average lower yield stress, $\sigma_y^l = 290$ MPa, were employed in order to perform meaningful comparisons.
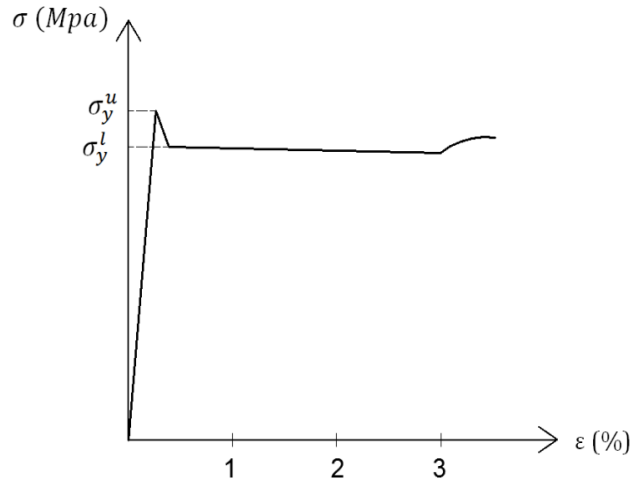
Figure 2.3: Typical stress-strain curve of the mild steel.

With respect to Blachut's examples, two approaches have been used in the present numerical analyses. In the first approach use has been made of an elastic-perfectly plastic flow theory (EPP flow theory). In the second approach recourse has been made to an isotropic non-linear hardening material model with an initial yield stress close to zero and a hardening curve based on the Ramberg-Osgood law (NLH flow theory). A detailed description of this implementation in the case of the flow theory of plasticity is given in Shamass et. al (2014).

It is worth noticing that, despite the very high value of the hardening parameter, the NLH flow theory cannot reproduce the elastic-perfectly plastic behaviour of the material undergoing monotonic loading, see Figure 2.4.

In order to compare the results from the flow theory with those from the deformation theory, the input parameters of the flow theory in the numerical analyses have been tuned so that the same stress-strain curve of the material as in the case of the deformation theory is obtained for the case of uniaxial stress and monotonic loading, to within a negligible numerical tolerance.
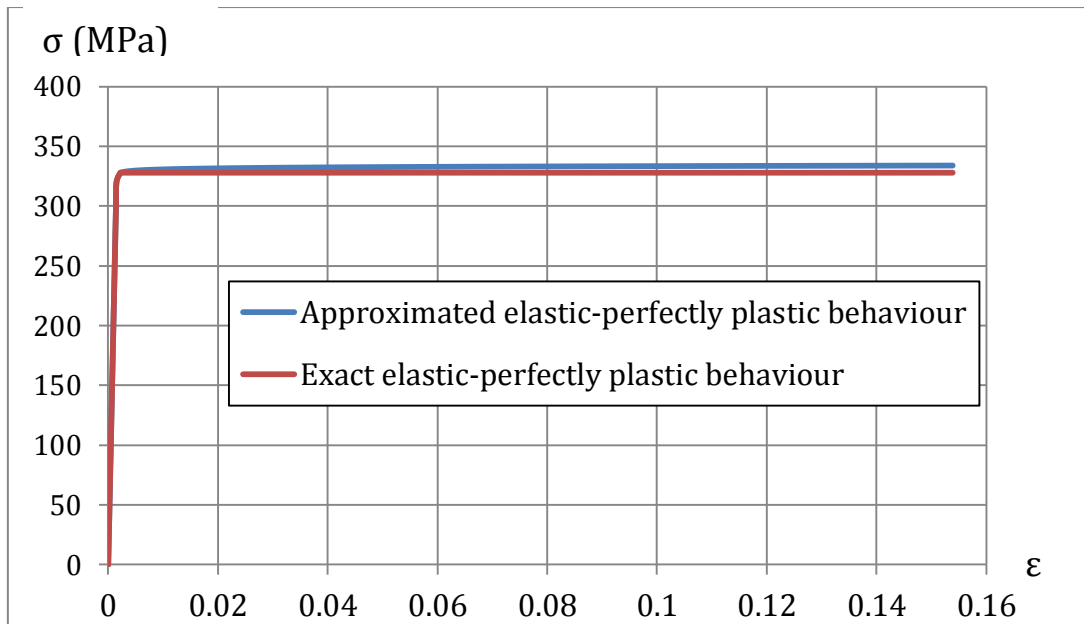
Figure 2.4: Comparison between the approximated and the exact elastic-perfect plastic material behaviour.

Giezen et al. (1991) reported stress-strain data from material tests on a number of strips machined from the original tubes of the sets A and.

With respect to Giezen 's examples, in the present study the material behaviour has been modelled by fitting the Ramberg-Osgood relation to the available data set, as shown in Figures 2.5-2.6.
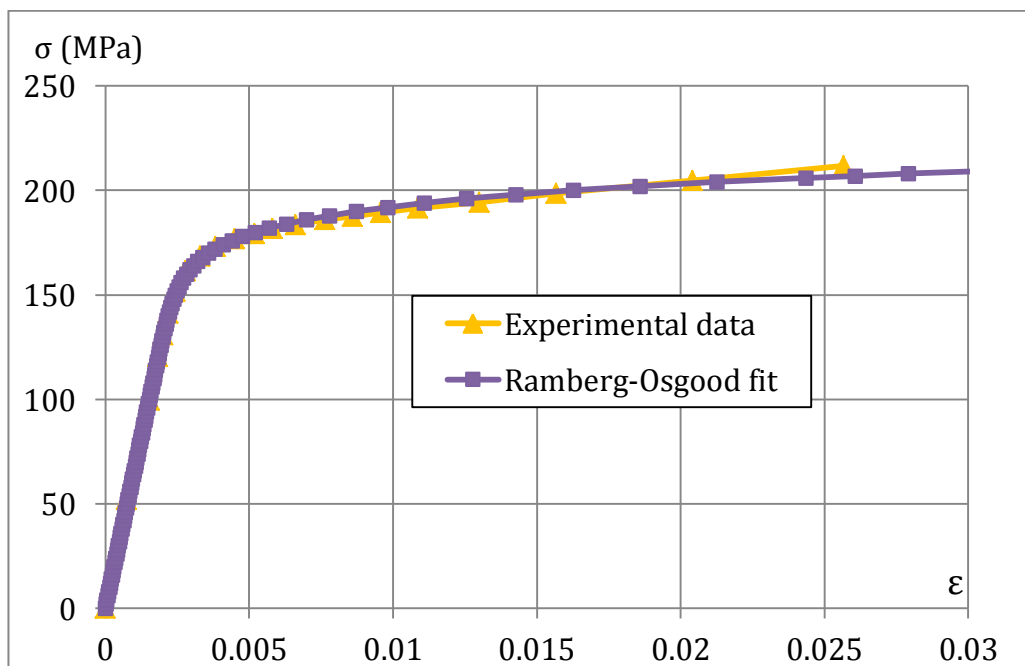
Figure 2.5: Ramberg-Osgood fit (Set A).
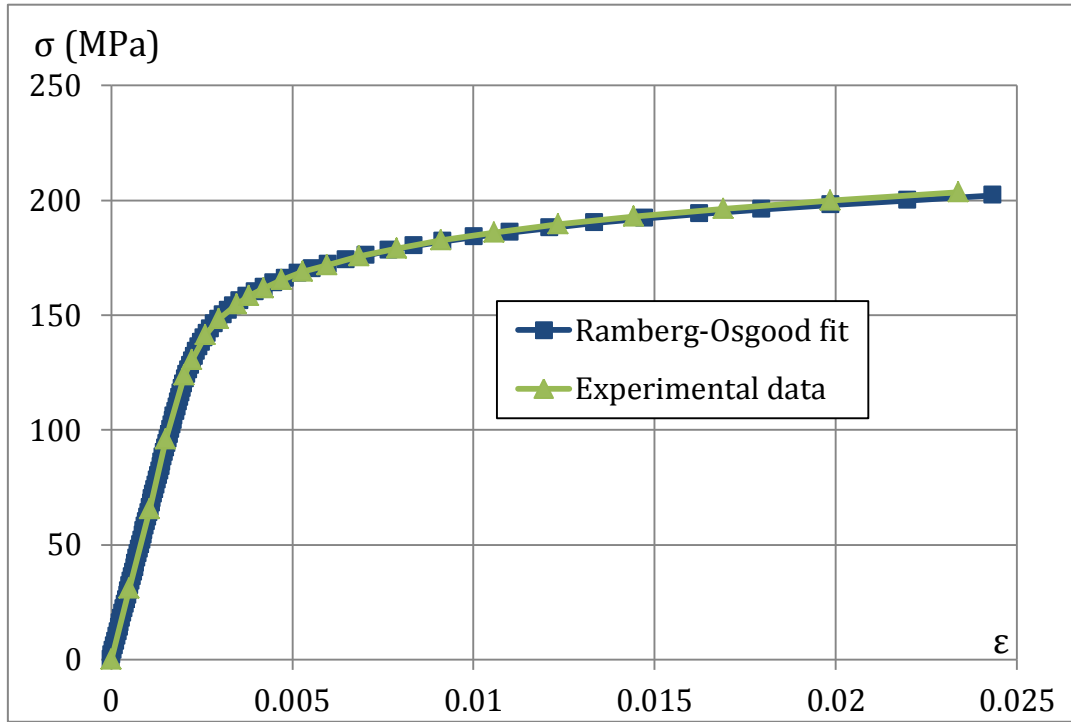
Figure 2.6: Ramberg-Osgood fit (Set B).

2.2.1 Adopted formulation of the deformation theory of plasticity

The formulation of the deformation theory of plasticity used in the numerical simulations has been obtained by extending the uniaxial Ramberg-Osgood law to the case of a multi-axial stress state using the von Mises formulation (J_2 theory). It results in the following path-independent relationship (Simulia, 2011):

$$E\boldsymbol{\varepsilon} = (1 + v)\operatorname{dev}\boldsymbol{\sigma} - (1 - 2v)\operatorname{sph}\boldsymbol{\sigma} + \frac{3}{2}\alpha\left(\frac{\sqrt{\frac{3}{2}}\|\operatorname{dev}\boldsymbol{\sigma}\|}{\sigma_y}\right)^{n-1}\operatorname{dev}\boldsymbol{\sigma} \qquad (2.2)$$

where $\boldsymbol{\varepsilon}$ and $\boldsymbol{\sigma}$ denote the strain and stress tensors, while $\operatorname{dev}\boldsymbol{\sigma}$ and $\operatorname{sph}\boldsymbol{\sigma}$ denote the deviatoric and spherical parts of the stress tensor, respectively.

Since the deformation theory of plasticity requires the same input values as the Ramberg-Osgood formula with the sole specification of the Poisson's ratio, the material constants of Table 2.6 have been used.

2.2.2 Adopted formulation of the flow theory of plasticity

The classical J_2 flow theory of plasticity with nonlinear isotropic hardening and in the small-strain regime (Simo and Hughes, 1998; Simulia, 2011) has been adopted in the numerical simulations. The theory is based on the additive decomposition of the spatial rate of the deformation tensor $\dot{\boldsymbol{\varepsilon}}$ into its elastic and plastic parts $\dot{\boldsymbol{\varepsilon}}_e$ and $\dot{\boldsymbol{\varepsilon}}_p$, respectively,

$$\dot{\boldsymbol{\varepsilon}} = \dot{\boldsymbol{\varepsilon}}_e + \dot{\boldsymbol{\varepsilon}}_p \tag{2.3}$$

The rate of the Cauchy stress tensor $\dot{\boldsymbol{\sigma}}$ is obtained from the elastic part of the strain tensor through the isotropic linear elastic relation

$$\dot{\boldsymbol{\sigma}} = 2G\dot{\boldsymbol{\varepsilon}}_e + \mu \operatorname{tr} \dot{\boldsymbol{\varepsilon}}_e \mathbf{I} \tag{2.4}$$

where G and μ are Lamé's elastic constants and $\mathbf{I}$ is the rank-2 identity tensor.
The von Misses yield function f is introduced in the form

$$f\big(\boldsymbol{\sigma}, \varepsilon_p^{eq}\big) = \|\operatorname{dev}\boldsymbol{\sigma}\| - \sqrt{\frac{2}{3}}\,\bar{\sigma}\big(\varepsilon_p^{eq}\big) \tag{2.5}$$

where $\bar{\sigma}$ represents the uniaxial yield strength that, in order to model nonlinear isotropic hardening, is assumed to be an increasing function of the equivalent plastic strain ε_p^{eq}, defined at time t as follows

$$\varepsilon_p^{eq}(t) = \int_{-\infty}^{t} \|\dot{\boldsymbol{\varepsilon}}_p(\tau)\|\, d\tau \tag{2.6}$$

The evolution of the plastic strain is given by the associate flow rule,

$$\dot{\boldsymbol{\varepsilon}}_p = \dot{\lambda}\left(\frac{\partial f}{\partial \boldsymbol{s}}\right)_{s=\operatorname{dev}\boldsymbol{\sigma}} \tag{2.7}$$

where $\dot{\lambda}$ is a plastic multiplier which must satisfy the complementarity conditions:

$$\dot{\lambda} \geq 0 \quad f\big(\boldsymbol{\sigma}, \varepsilon_p^{eq}\big) \leq 0 \qquad \dot{\lambda}\, f\big(\boldsymbol{\sigma}, \varepsilon_p^{eq}\big) = 0 \tag{2.8}$$

2.3 Large displacement formulation

The numerical analyses have been performed in the realm of large-strains by using spatial co-rotational stress and strain measures and a hypo-elastic relation between the rates of stress and elastic strain (Simulia, 2011). It is worth noticing that in the past this

approach has been the subject of a debate because hypo-elastic laws may occasionally tend to lead to fictitious numerical dissipation (Simo and Hughes, 1998). However, the adopted large-strain formulation is widely implemented in many commercial codes, including ABAQUS, and it is generally accepted that the hypo-elasticity of the formulation has limited influence on the results because, even when strains are large, the elastic part of the strain is typically still very small and close enough to the limit where hypo-elastic and hyper-elastic formulations coincide (Simo and Hughes, 1998).

In order to follow the structural response beyond the buckling load, that is a limit point when load control is applied, the Riks arc-length method (Riks, 1979) has been used in the version implemented in ABAQUS (Simulia, 2011). In this method both the nodal displacement increments, Δu, and the increment, $\Delta\lambda$, of the load multiplier are assumed unknown in each increment. The Riks' formulation iterates along a hyperplane orthogonal to the tangent of the arc-length from a previously converged point on the equilibrium path (Falzon, 2006).

In the present study, the external pressure is set as $\lambda\, p_0$, where p_0 denotes a reference inward external pressure and λ is a scalar multiplier. The critical load is determined by the point at which the load-arc length curve reaches a maximum.

The bifurcation point is the intersection of secondary and primary paths, which are the pre-buckling and post buckling paths, respectively. To avoid such discontinuous response at bifurcation, it is common to introduce geometric imperfections in order to remove bifurcation points (Falzon, 2006; Simulia, 2011). In this way, the post-buckling problem analysed using Riks method will turn into a problem with a continuous response. The critical point determined on the equilibrium path is the limit point and there is no bifurcation prior to collapse. The choice of the size of the imperfection and its shape is discussed in later sections. Furthermore, if analyses are conducted with progressively reduced size of the imperfection, the limit point found in those with the smallest amount of imperfections; say 0.05% or 0.1% of the thickness turns out to be a good approximation of the bifurcation load (Bushnell, private communication). This method is used later in Section 5.3.

2.4 Description of imperfections

Accounting for imperfections has been achieved by scaling and adding buckling eigenmodes to a perfect geometry in order to create a perturbed initial geometry. The scaling factor has been set as a percentage of the shell thickness, *t*. The analyses have been conducted for an imperfection amplitude equal to 1% of the thickness, as experimentally measured by Blachut et al. (1996).

The choice of linear elastic eigenmodes used to generate the imperfect models was made with the aim of choosing those with the same number of circumferential waves that were found experimentally in the post-buckling path. Except for specimen M2, for which a buckling mode with 3 waves was reported, Blachut et al. (1996) did not report the observed failure modes of the other cylinders. However, they did report that the number of circumferential waves observed from the test varied from 3 waves for high values of axial tensile load to 6 waves for pure applied external pressure. Therefore, for very small values of the axial load such as in specimen S2, the fifth eigenmode with 6 waves was used; for specimen M2 and for the others which were tested with very high tensile loads, the eigenmode corresponding to 3 waves was used; for the other specimens subject to intermediate smaller or larger tensile loads, the eigenmodes with 5 or 4 waves were used, respectively. This is summarised in Table 2.7, which shows the eigenmode number used to generate the shape of imperfection in the FE models for each specimen together with the associated number of circumferential waves (see Figure 2.7).

On the other hand, Giezen et al. (1991) reported the buckling failure modes found experimentally, as illustrated in Tables 2.4-2.5. Hence, for these cases the eigenmodes used to generate the imperfections are those with the same number of waves found experimentally, with a single wave in the longitudinal direction. Accordingly, the eigenmodes with five circumferential waves have been chosen to generate initial imperfection's shape for specimens SP.1 to SP.4 in Set A and those with four waves have been chosen for the rest of the specimens (see Figure 2.8). The analyses have been conducted for an imperfection amplitude equal to 10% of the thickness for both Set A and B, as experimentally measured by Giezen et al. (1991).

In all the cases the linear buckling analysis has been conducted assuming linear elastic material behaviour and small displacements, under constant axial tensile loading.

It is worth pointing out that existing results show that it is not universally true for geometrically imperfect structures to fail by collapse at a reduced magnitude of load. In fact, Blachut and Galletly (1993) observed that the elastic buckling load of externally pressurized torispheres was not affected by local flattening with small amplitudes and this fact was verified experimentally. Actually, the limit carrying load of shells of revolution is known to exhibit complex phenomena including mode switching and interaction and many analyses of the non-axisymmetric buckling deformation of spherical domes suggest that the observed deformation at collapse is mostly determined by the form of the imperfections, rather than by their magnitude.

This seems to be hardly the case with the circular cylindrical shells object of the present study, especially in the case of non-proportional loading. In fact, apart from the observation that the behaviour described by Blachut and Galletly tends to depend on the rise of the torispheres, a geometric characteristic which does not pertain to cylinders, in the performed numerical analyses, the R/t ratio of the cylinders was about 25, placing the buckling in a substantially pure plastic range, where imperfect shells are prone to show a reduced collapse load with respect to perfect ones. As an additional point, Figures 5.2 and 5.4 show that the plastic buckling resistances of the cylinders under analysis are actually sensitive to imperfection amplitudes.

Specimens	S1	S2	S3	S4	S5	S6	S7
Eigenmode number	3	5	3	1	3	3	1
Number of circumferential waves	4	6	4	5	4	3	5

Specimens	M2	M12	M7	L4	L8
Eigenmode number	7	7	7	1	3
Number of circumferential waves	3	3	3	4	3

Table2.7: Number of circumferential waves used to generate imperfections in the FE modelling for the specimens tested by Blachut et al. (1996).
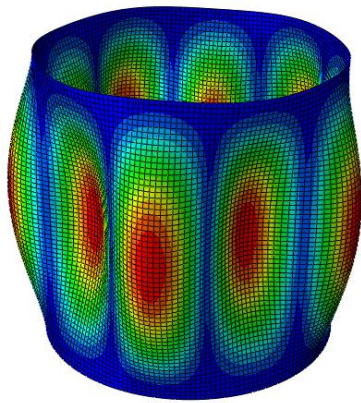
First eigenmode for S4 cylinder   Seventh eigenmode for M2 cylinder
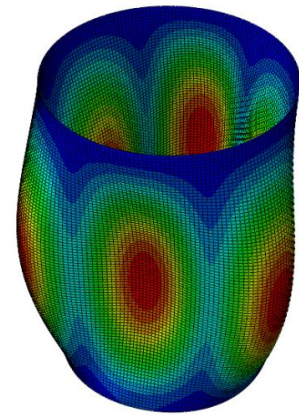
Figure 2.7: Buckling eigenmodes used in the simulation of Blachut's tests to account for initial imperfections.
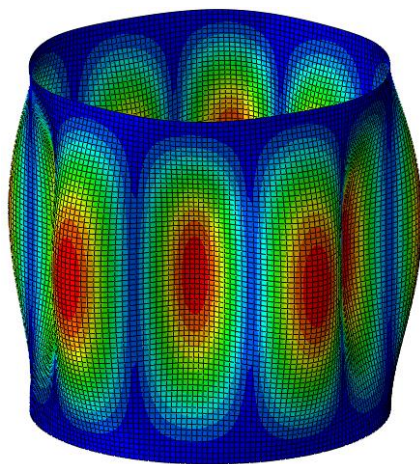
First eigenmode for SP.1 (Set A) cylinder   Fifth eigenmode for SP.1 (Set B) cylinder
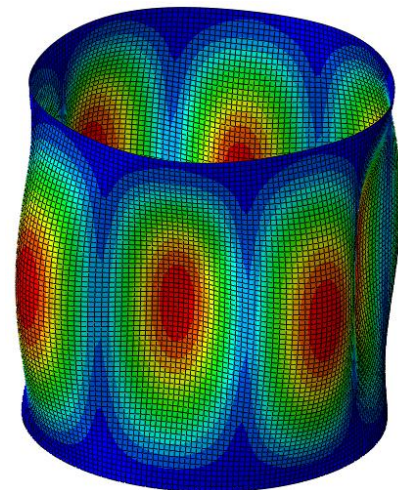
Figure 2.8: Buckling eigenmodes used in the simulation of Giezen's tests to account for initial imperfections.

3. Finite-element results for the experiments in Blachut et al. (1996)

3.1 Comparison of the numerical results with experimental results

The buckling pressures, based on the deformation theory, the EPP flow theory and the NLH flow theory of plasticity, have been calculated for different specimen geometries, axial tensions and both values of the average yield stress. The results are illustrated in Figures 3.1 and show that the buckling pressures predicted by the NLH

flow theory and by the deformation theory of plasticity are extremely close to each other.

The calculated buckling pressures based on the flow theory and the deformation theory in conjunction with the upper value of the yield stress are in better agreement with experimental results for the specimens S2, S3, S5, S7, M2, M12 ,M7, and L4. The calculated buckling pressures based on the flow theory and the deformation theory in conjunction with the lower value of the yield stress are in better agreement with experimental results for the specimens S1, S4, S6, and L8.
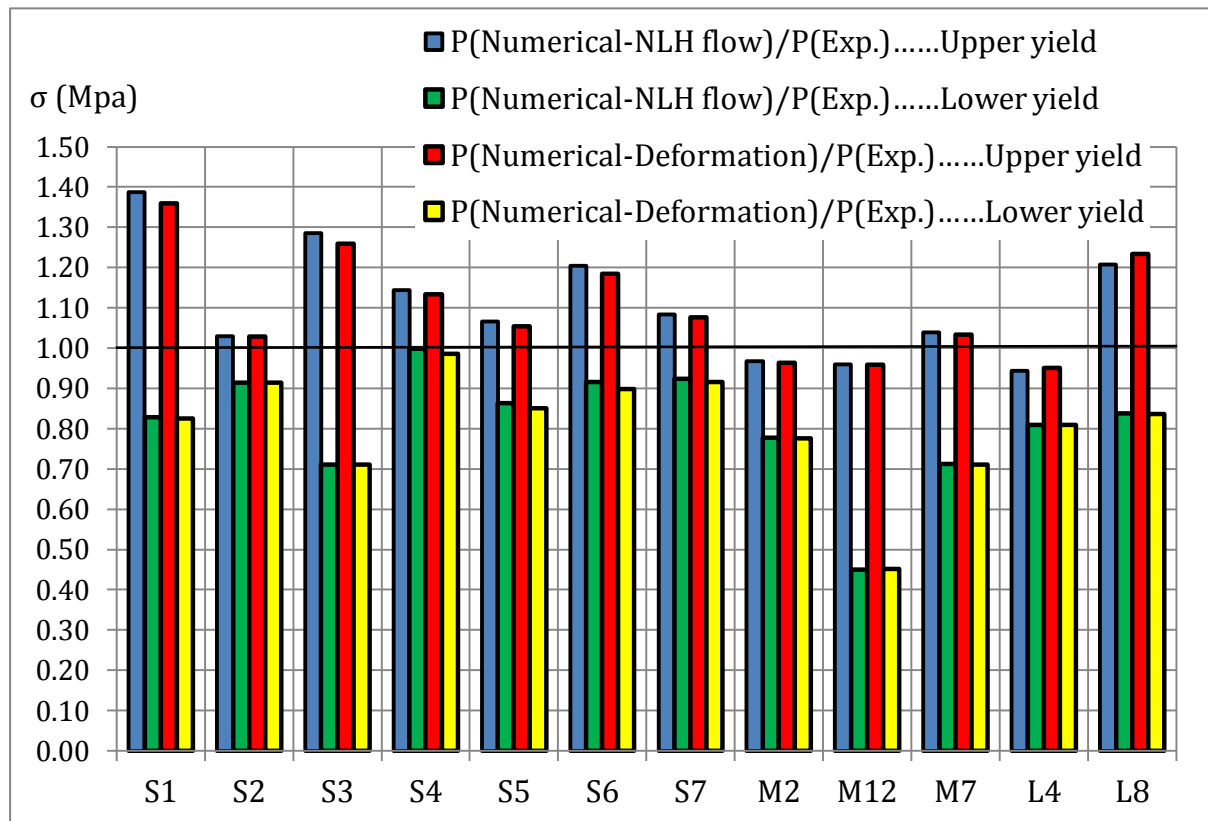
Figure3.1: Comparison between experimental and numerical results for both the deformation theory and the NLH flow theory of plasticity.

Figure 3.2 shows the plots of the external pressure vs the radial displacement of a point at the middle section of the cylinders resulting from both the flow and the deformation theory of plasticity for different specimens. It can be noticed that the curves predicted by the flow theory lay above the curves predicted by the deformation theory in most cases.

Figures 3.3-3.4 show the predicted circumferential and meridian plastic strains at the onset of buckling according to the flow and deformation theory of plasticity. It can be observed that the differences in the predictions increase with the intensification of the applied tensile load.

Figures 3.3-3.4 show that, according to the proposed modelling, both plasticity theories succeed in predicting buckling with physically acceptable plastic strains for all specimens. In fact, although the maximum plastic strains calculated at the buckling pressure in meridian and circumferential directions and predicted by the NLH flow theory of plasticity are larger than those predicted by the deformation theory, they result still acceptable for all specimens with $L/D \approx 1$. Additionally, Tables 3.1-3.3 show that meridian and circumferential plastic strains predicted using the flow theory of plasticity are physically realistic, being smaller than 1.5%, with the exception of specimens S1, S3 and S6 in Table 3.3, with still display values largely below 5%. From this standpoint all the plastic buckling pressures shown in Figure 3.1 and calculated using the flow theory can be thus considered physically acceptable.
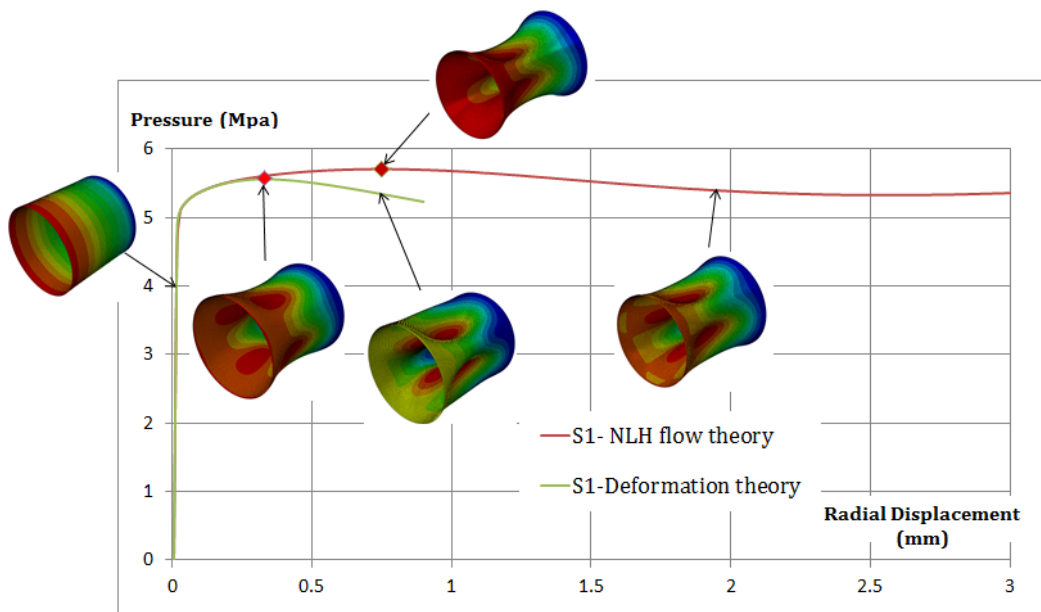
(a) External pressure versus radial displacement for specimen S1

20
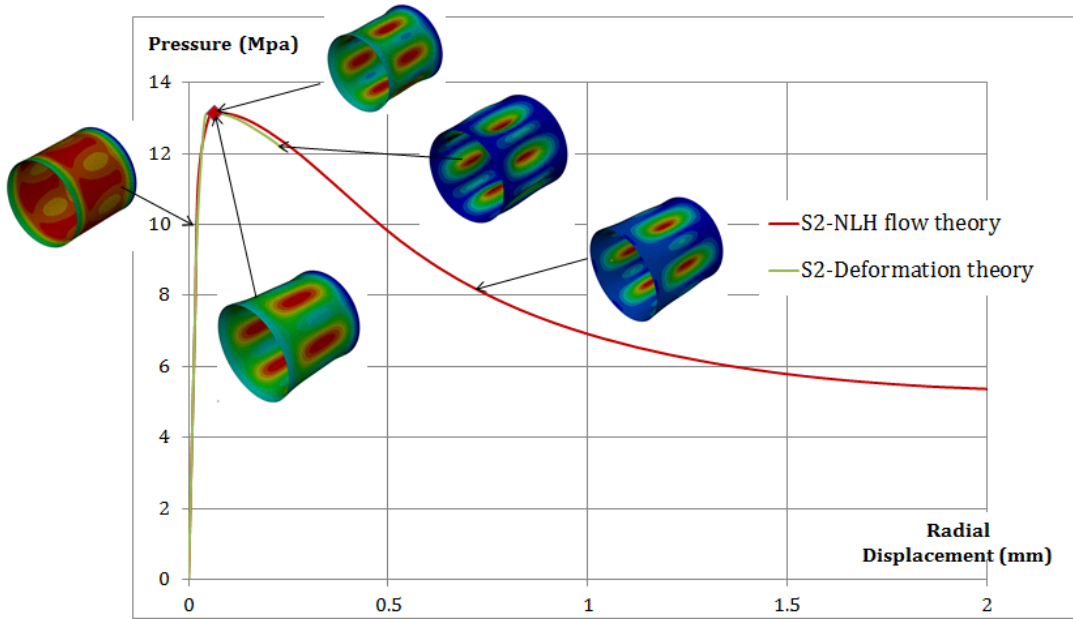
(b) External pressure versus radial displacement for specimen S2
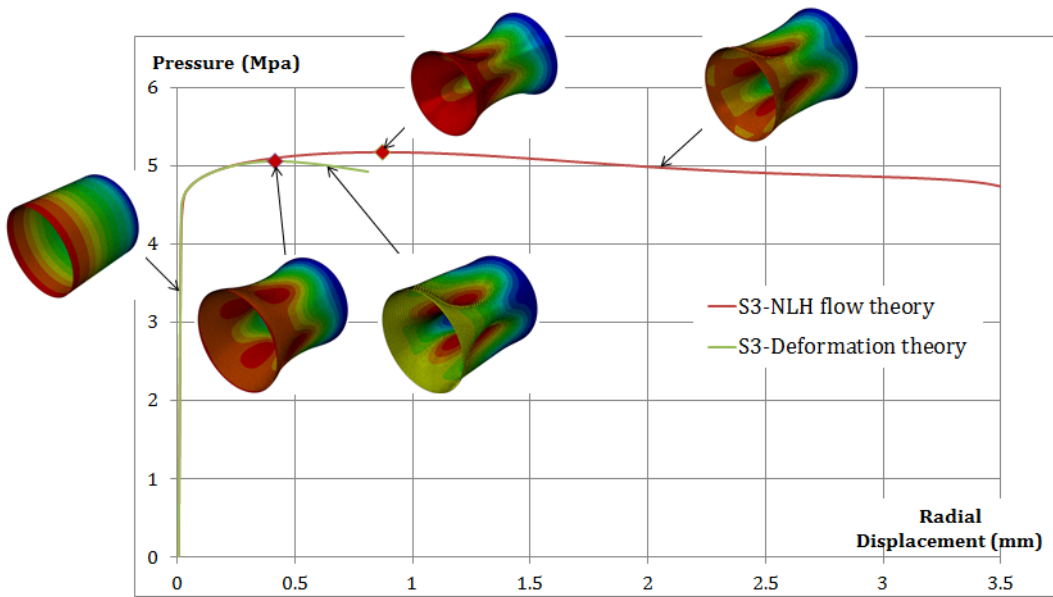
(c) External pressure versus radial displacement for specimen S3

21
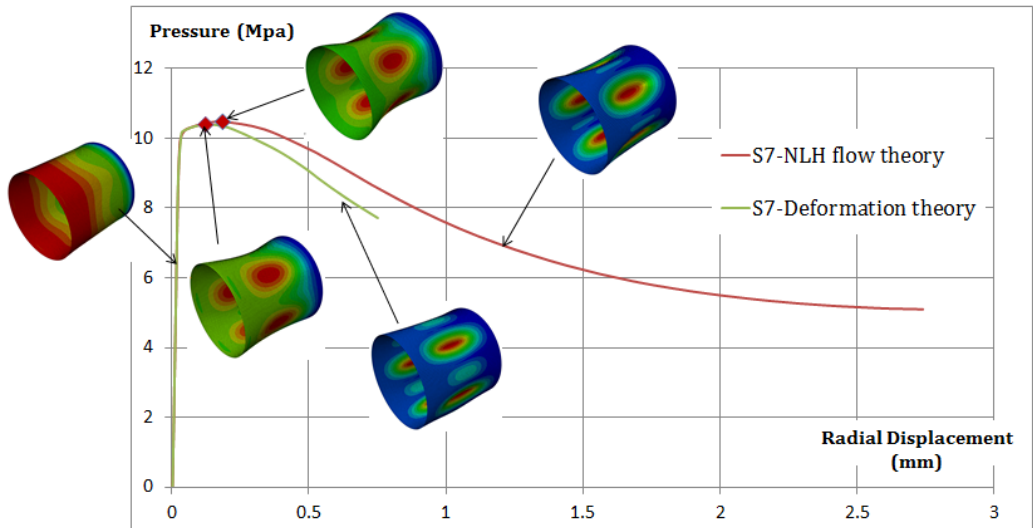
(d) External pressure versus radial displacement for specimen S7
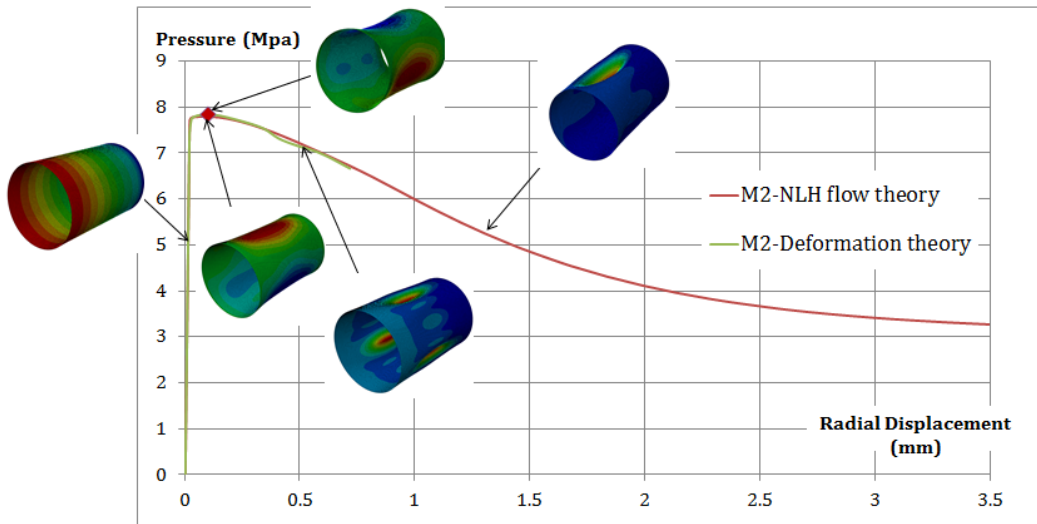
(e) External pressure versus radial displacement for specimen M2

22
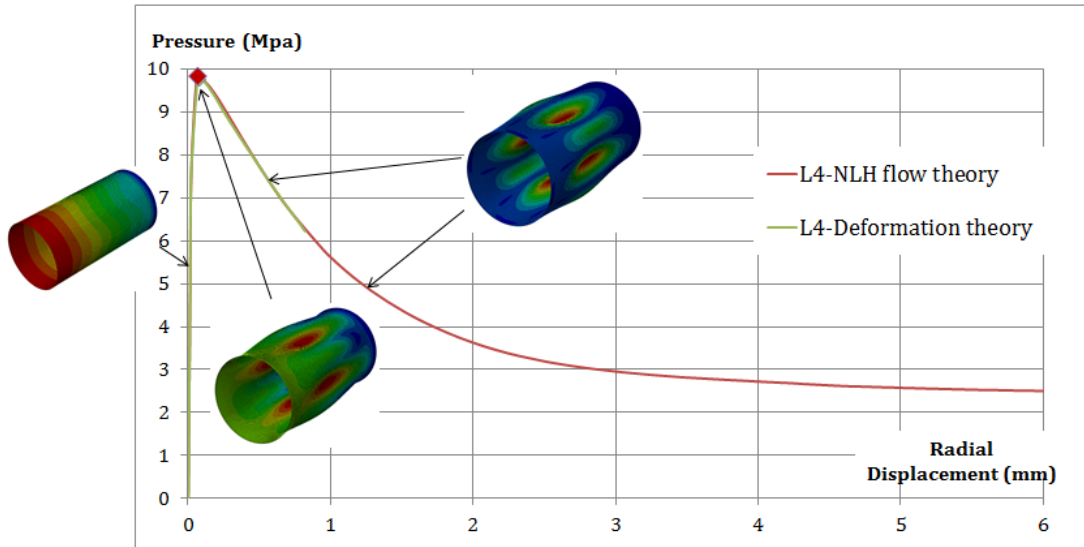
(f) External pressure versus radial displacement for specimen L4

Figure 3.2: External pressure vs. radial displacement curves for specimens (a) S1, (b) S2, (c) S3, (d) S7, (e) M2 and (f) L4 (upper value of the yield stress) showing the buckling response, ultimate external pressure and deformation modes before, after and at the limit pressure load (colours indicating the total deformation).
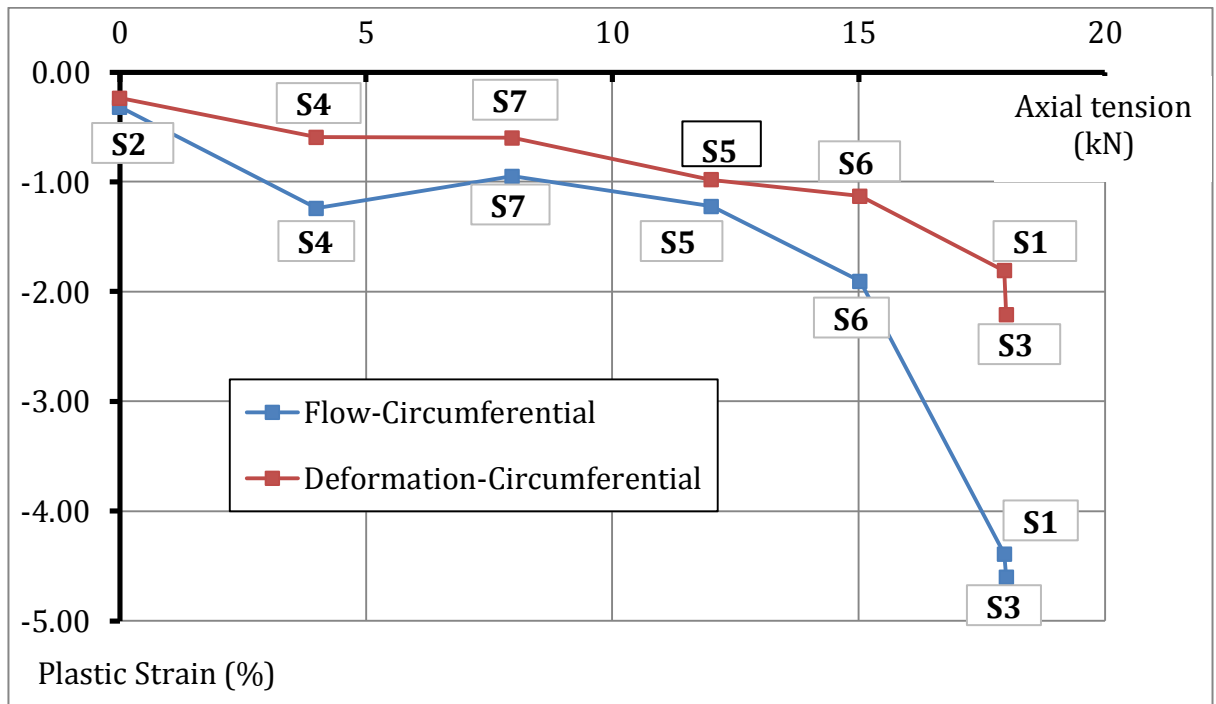
Figure 3.3: Maximum circumferential plastic strains at the mid-section of the cylinders under combined loading ($L/D \cong 1$), calculated using the upper value of the yield stress.
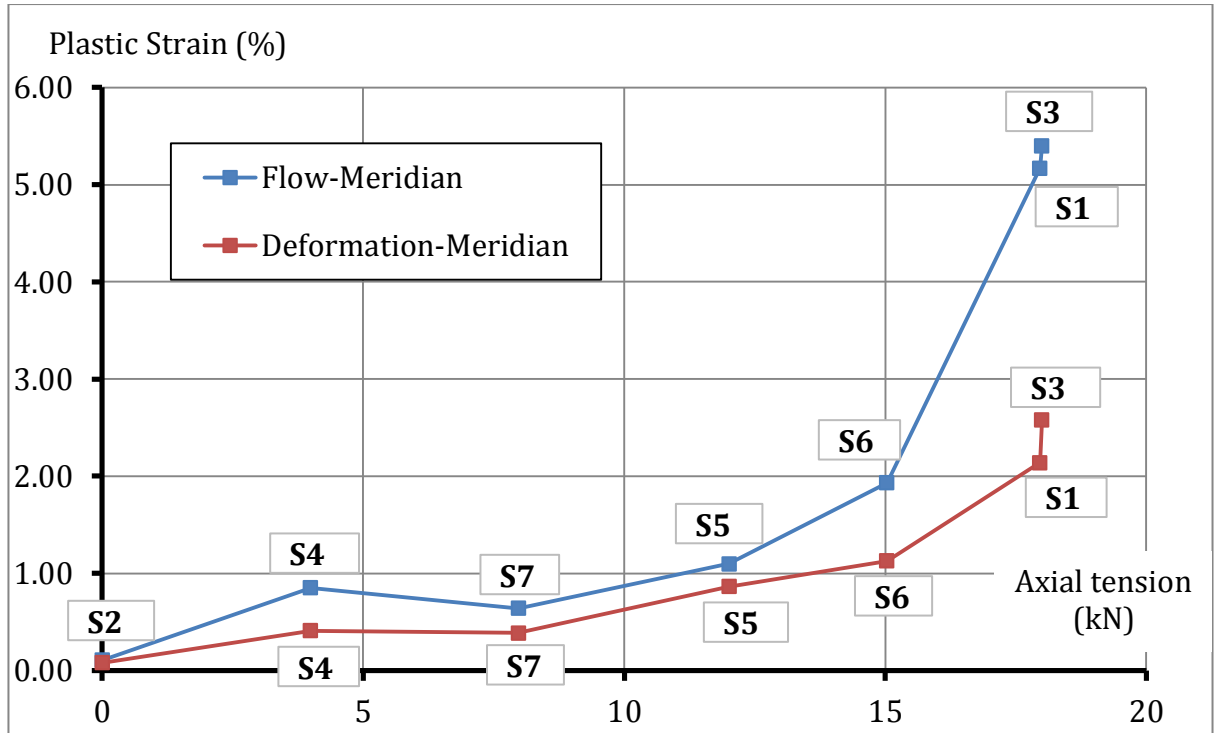
Figure 3.4: Maximum meridian plastic strains at the mid-section of the cylinders under combine loading ($L/D \cong 1$), calculated using the upper value of the yield stress.

Spec	M2		M12		M7		L4		L8	
	C	M	C	M	C	M	C	M	C	M
S=0	-0.028	0.320	-0.030	0.320	-0.027	0.242	-0.021	0.176	-0.0245	0.205
S=0.25	-0.453	0.403	-0.580	0.750	-0.380	0.404	-0.065	0.044	-0.210	0.231
S=0.5	-0.679	0.603	-0.960	1.250	-0.638	0.660	-0.151	0.087	-0.309	0.318
S=0.75	-0.453	0.403	-0.640	0.866	-0.380	0.404	-0.065	0.037	-0.210	0.223
S=1	-0.028	0.320	-0.030	0.320	-0.027	0.242	-0.021	0.176	-0.0245	0.205

Table 3.1: Maximum plastic strains (%) at the buckling at different sections of the cylinders (S=x/L), according to the NLH flow theory of plasticity and using the upper value of the yield stress (C-circumferential direction; M-meridian direction).

Spec	M2		M12		M7		L4		L8	
	C	M	C	M	C	M	C	M	C	M
S=0	-0.023	0.266	-0.026	0.454	-0.207	0.220	0.018	0.160	-0.020	0.190
S=0.25	-0.330	0.298	-0.734	0.961	-0.261	0.273	-0.047	0.032	-0.138	0.150
S=0.5	-0.480	0.420	-1.268	1.656	-0.417	0.421	-0.127	0.071	-0.179	0.182
S=0.75	-0.330	0.298	-0.734	0.961	-0.261	0.273	-0.047	0.032	-0.138	0.150
S=1	-0.023	0.266	-0.026	0.454	-0.207	0.220	0.018	0.160	-0.020	0.190

Table 3.2: Maximum plastic strains (%) at the buckling at different sections of the cylinders (S=x/L), according to the deformation theory of plasticity and using the upper value of the yield stress.

Spec.	NLH flow theory		Deformation plasticity	
	Circumferential	Meridian	Circumferential	Meridian
S1	-2.66	4.00	-2.96	4.52
S2	-0.36	0.13	-0.28	0.09
S3	-2.63	4.14	-2.06	3.30
S4	-1.25	0.88	-0.49	0.34
S5	-1.80	1.54	-0.91	0.88
S6	-2.60	2.93	-1.66	1.77
S7	-1.00	0.77	-0.67	0.51
M2	-0.94	0.89	-0.56	0.53
M12	-0.52	0.84	-0.62	1.00
M7	-0.83	1.02	-0.83	0.94
L4	-0.13	0.08	-0.86	0.14
L8	-0.57	0.69	-0.37	0.44

Table 3.3: Maximum plastic strains (%) at the buckling pressure based on the flow theory and the deformation theory of plasticity, calculated using lower value of yield stress.

3.2 Comparison of the FE results with the numerical results by Blachut et al. (1996)

Blachut et al. (1996) conducted numerical analyses of their experimental tests using the code BOSOR5. In their investigation they looked for the plastic buckling pressure and scrutinized which plasticity theory used in BOSOR5 seemed to better agree with the

test results. The most significant finding was that the maximum plastic strains for most of numerically tested cylinders as predicted by the flow theory were an order of magnitude greater than those predicted by the deformation theory of plasticity. As a consequence, they concluded that the flow theory predictions (including buckling pressures) were physically unrealistic and incorrect, particularly when $D/L \approx 1$.

This finding is in contrast with the numerical results from the present study, as shown in Tables 3.1-3.3 and Figures 3.3-3.4. In fact, the presented numerical findings show that the flow theory can predict buckling within physically acceptable plastic strains.

Figure 3.5 shows that although the flow theory used by Blachut et al. (1996) using BOSOR5 and the upper yield material stress failed to predict buckling for all selected specimens except for S2 and L4, the present numerical investigation based on the flow theory succeeded in predicting buckling for all specimens with physically acceptable plastic strains. Therefore, according to the presented results both plasticity theories can reasonably predict plastic buckling pressure values. Moreover, the plastic buckling pressures yielded by the FE analyses using the deformation theory are extremely close to those calculated by Blachut et al. (1996).
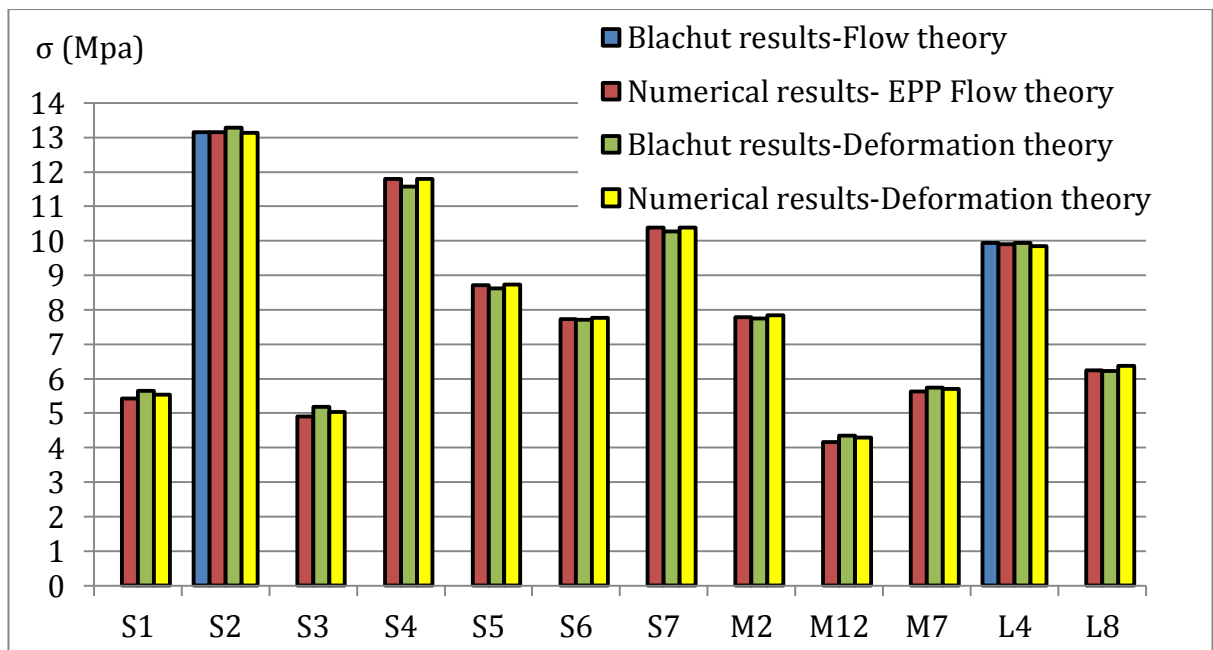
Figure 3.5: Comparison of Blachut et al. (1996) with present numerical predictions for both the flow and deformation theories of plasticity, using the upper yield stress.

Blachut et al. (1996) also reported the plastic strains obtained by means of the flow and deformation theory of plasticity for an axial tensile load of 10 kN on the basis of the upper yield stress ($\sigma_{yp}^u = 328\,\text{MPa}$), for specimens with average geometry $D/L = 0.98$ and $D/L = 1.47$. The comparison with the present numerical analyses, presented in Table 3.4(a), shows that plastic buckling pressure predicted by Blachut et al. (1996) and based on the flow theory is larger than the one predicted by the deformation theory by about 34%. Moreover, the maximum predicted plastic strains seemed unacceptable and this fact led Blachut et al. (1996) to agree only with the predictions from the deformation theory. However, the present numerical investigations show that the plastic buckling pressures predicted by the flow theory are close to those by the deformation plasticity, see Tables 3.4(a)-3.4(b). Moreover, the maximum plastic strains resulting from the FE analyses using the flow theory and the deformation theory result different from those reported in Blachut et al. (1996) and physically acceptable. For instance, the maximum plastic strains in meridian and circumferential directions, shown in Table 3.4(a) calculated by Blachut et al. (1996) according to the flow theory are 63% and -19.42%, respectively, while the maximum plastic strains given by the present study are 0.7% and -0.85%.

(a) $L/D = 0.98$

	Flow theory (Blachut et al.,1996)		Deformation theory (Blachut et al., 1996)	
Buckling pressure	12.7		9.52	
Maximum plastic strains (%)	**Meridian**	**Circumferential**	**Meridian**	**Circumferential**
S=0	63.08	-0.049	1.273	-0.034
S=0.25	13.11	-13.652	0.193	-0.213
S=0.5	18.57	-19.42	0.390	-0.439
S=0.75	13.11	-13.652	0.193	-0.213
S=1	63.08	-0.049	1.273	-0.034

Plastic strains results obtained by Blachut et al. (1996) using the flow theory and the deformation theory of plasticity, L/D=0.98

	EPP flow theory Our numerical analysis		Deformation theory Our numerical analysis	
Buckling pressure	9.53		9.38	
Maximum plastic strains (%)	**Meridian**	**Circumferential**	**Meridian**	**Circumferential**
S=0	0.330	-0.029	0.30	-0.0233
S=0.25	0.327	-0.423	0.249	-0.34
S=0.5	0.700	-0.85	0.54	-0.675
S=0.75	0.327	-0.423	0.249	-0.34
S=1	0.330	-0.029	0.30	-0.0233

Plastic strains results obtained by present numerical analysis using the flow theory and the deformation theory of plasticity, L/D=0.98

(b) $L/D = 1.47$

	Flow theory (Blachutetal.,1996)		Deformation theory (Blachutetal.,1996)	
Buckling pressure	8.92		8.8	
Maximum plastic strains (%)	**Meridian**	**Circumferential**	**Meridian**	**Circumferential**
S=0	1.667	-0.034	0.406	-0.032
S=0.25	0.462	-0.523	0.047	-0.054
S=0.5	0.785	-0.888	0.005	-0.005
S=0.75	0.462	-0.523	0.047	-0.054
S=1	1.677	-0.034	0.406	-0.032

Plastic strains results obtained by Blachut et al. (1996) using the flow theory and the deformation theory of plasticity, L/D=1.47

	EPP flow theory Our numerical analysis		Deformation theory Our numerical analysis	
Buckling pressure	8.077		8.079	
Maximum plastic strains (%)	**Meridian**	**Circumferential**	**Meridian**	**Circumferential**
S=0	0.1700	-0.0212	0.1750	-0.0188
S=0.25	0.0900	-0.1160	0.0880	-0.1150
S=0.5	0.1130	-0.1550	0.1100	-0.1500
S=0.75	0.0900	-0.1160	0.0880	-0.1150
S=1	0.1700	-0.0212	0.1750	-0.0188

Plastic strains obtained by present numerical analysis using the flow theory and the deformation theory of plasticity, L/D=1.47

Table 3.4: Comparison between plastic strains obtained by Blachut et al. (1996) and those by the present numerical analysis using the flow theory and the deformation theory of plasticity.

4. Comparison of the FE results with the results by Giezen et al. (1991)

Giezen et al. (1991) conducted numerical analyses on the set of cylindrical specimens tested by means of the code BOSOR5 and an axisymmetric shell formulation. They too observed that the results from the deformation theory results were in better agreement with the experimental ones than those predicted by the flow theory. Moreover, the flow theory seemed to display a stiffening character, in the sense that the buckling load increased with the axial tensile load. This was in contrast with their experimental findings.

The present numerical analyses show that both the flow and the deformation theory display a softening character with the increase in the axial tensile load (Figures 4.1-4.2). Furthermore, Figures 4.1-4.2 show that the difference between the flow and the deformation theory predictions increases with the intensification of the non-proportionality of the load while become almost negligible when the loading tends to be proportional (i.e. when the tensile load tend to become negligible).
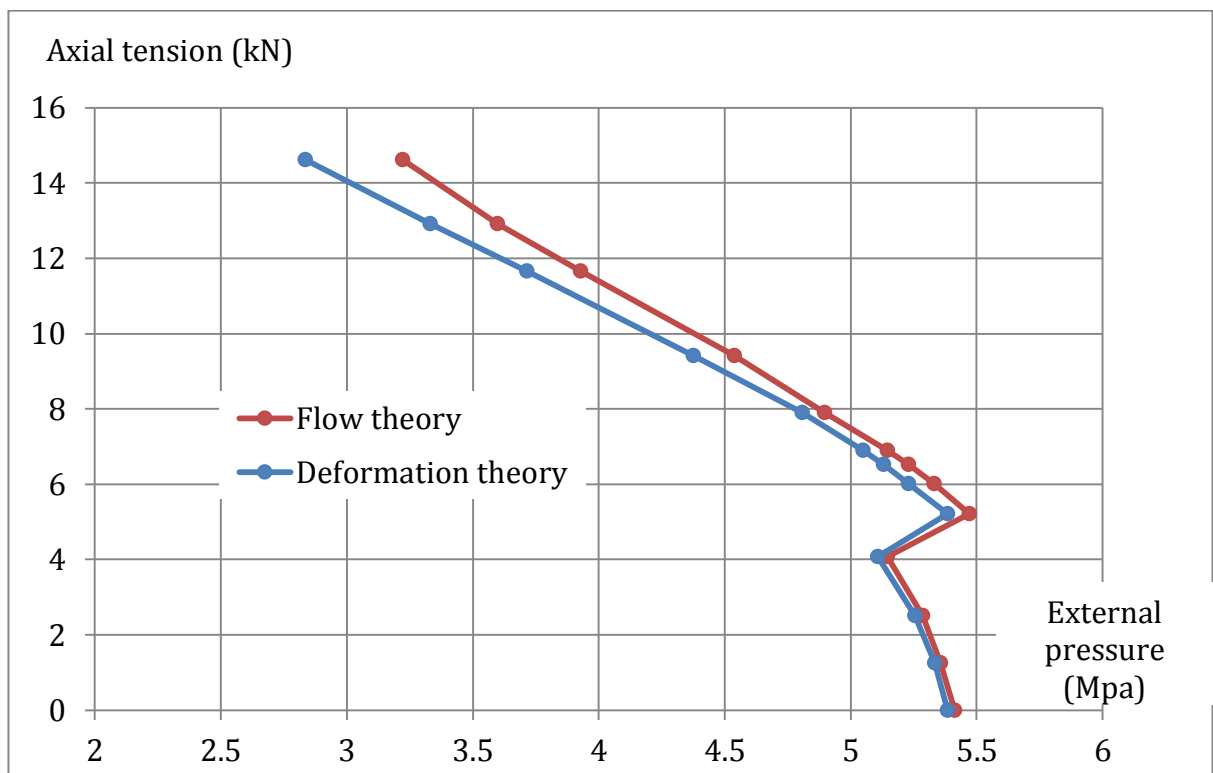
Figure 4.1: External pressure vs axial load – present numerical results (Set A)
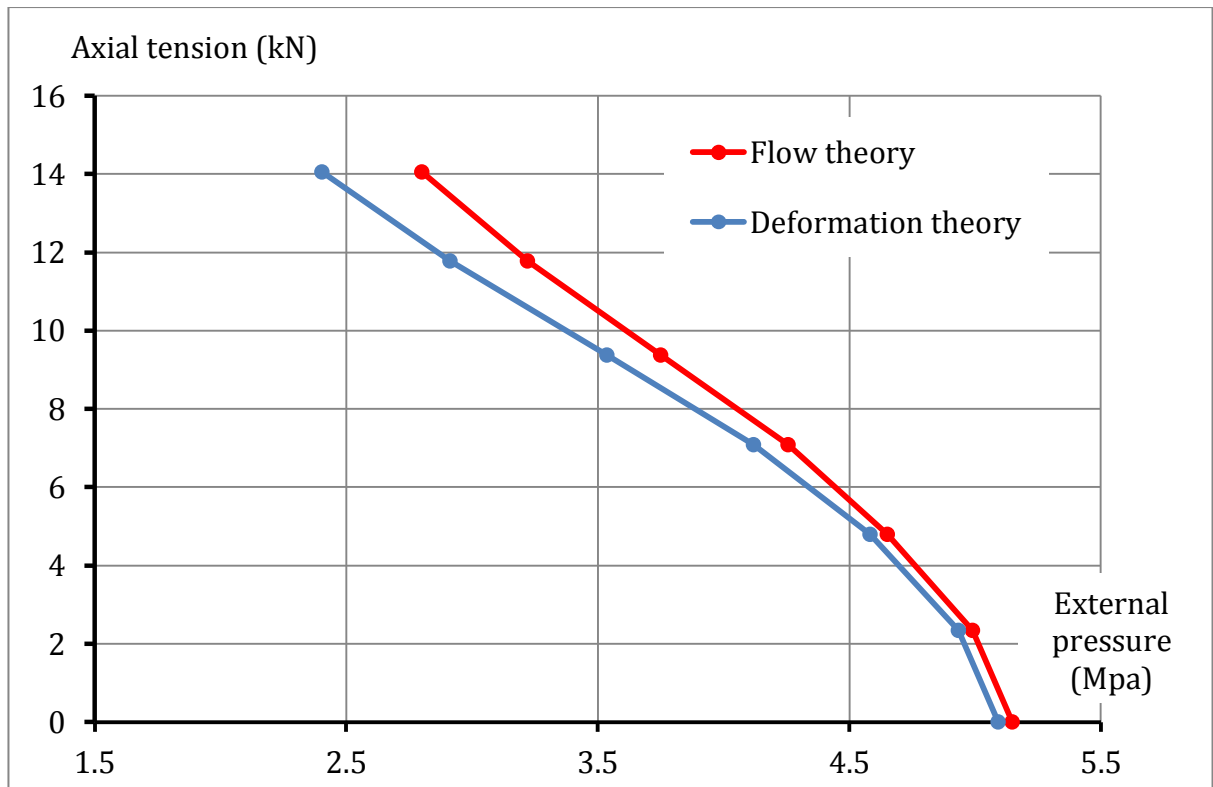
Figure 4.2: External pressure vs axial load – present numerical results (Set B).

Figures 4.3-4.4 show that the results calculated using the flow theory are in better agreement with the test results than those using the deformation theory for all specimens except SP.7 in set B, for which the flow theory and the deformation theory over-predict the buckling pressure by 37% and 18%, respectively. Figure 4.3 shows that the buckling pressures calculated using both the flow and deformation theories tend to fall short of the experimental values. In the case of the flow theory, the discrepancy between the numerical and experimental values ranges between 4% and 20% while in the case of the deformation theory the discrepancy ranges between 6% and 30%. On the other hand, Figure 4.4 shows that the differences with the experiment in the case of the flow theory range between 0.2% and 7.5%, with the exception of SP.7, while in the case of the deformation theory the differences range between 1.2% and 7.2%. Overall, it can be concluded that, according to the present analyses, the flow theory succeeds in predicting buckling pressure in all cases except one, with a deviation from the test results which is generally below 20% and in many cases below 10%.
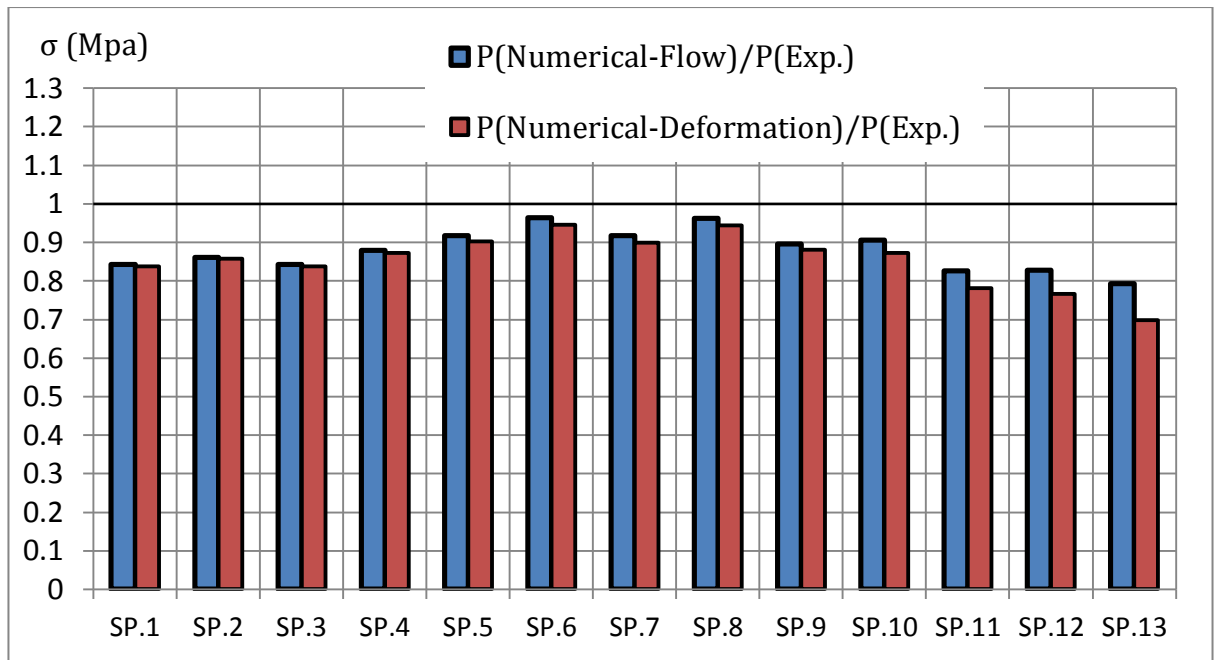
Figure 4.3: Comparison between numerical and test results (Set A).
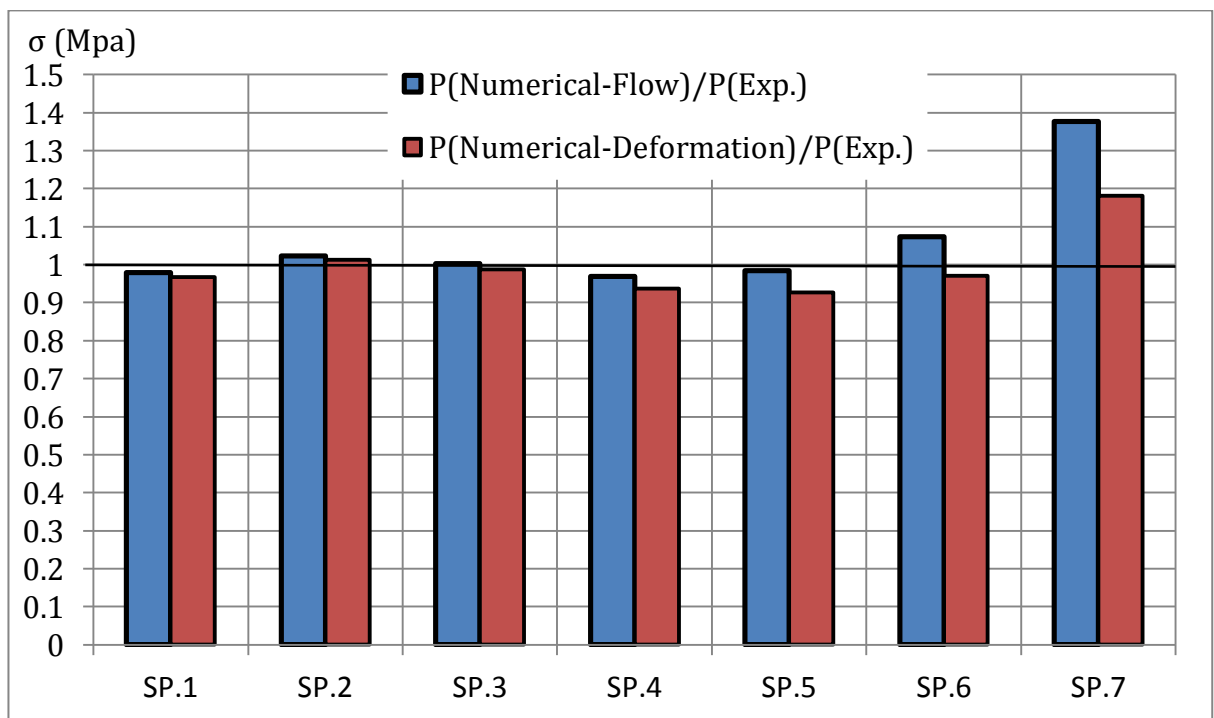
Figure 4.4: Comparison between numerical and test results (Set B).

A comparison between the flow and the deformation theory predictions in terms of plastic strains at the onset of buckling can be also interesting. The plastic strains from the deformation theory seem generally less sensitive to the non-proportionality of loading than those predicted by the flow theory for moderate values of axial tension, as

shown in Figures 4.5-4.8. The plastic strains calculated using the flow and deformation theory are very close for low values of the tensile load but the discrepancies increase with the biaxial loading.
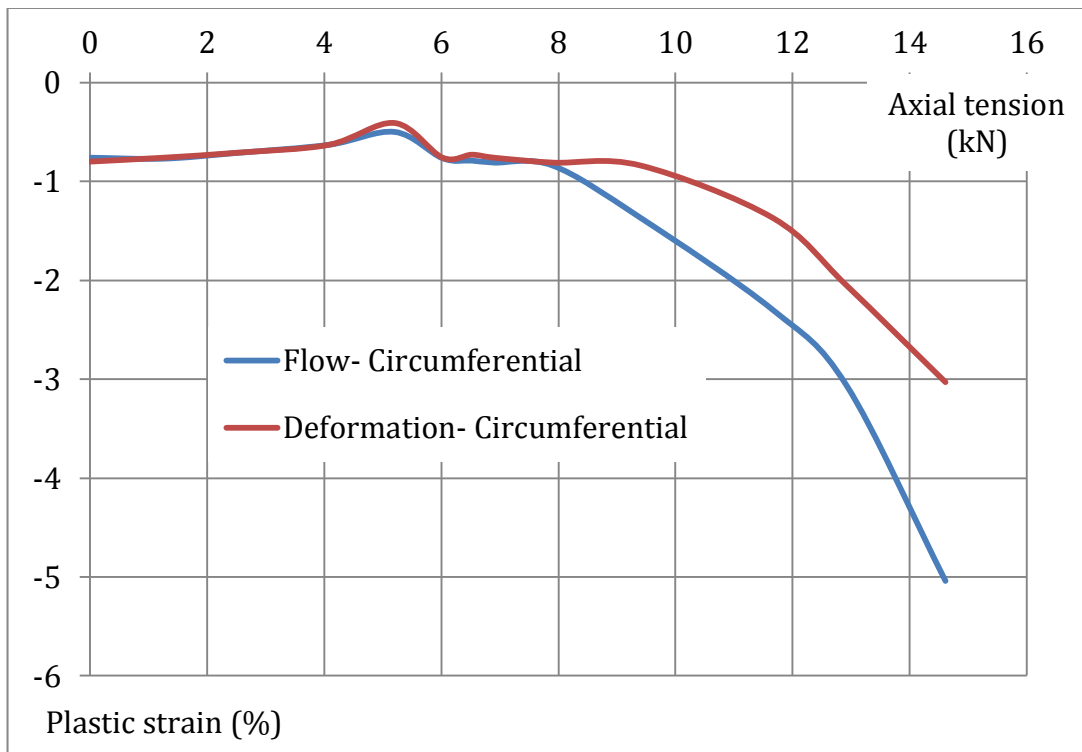
Figure 4.5: Maximum circumferential plastic strains (Set A).
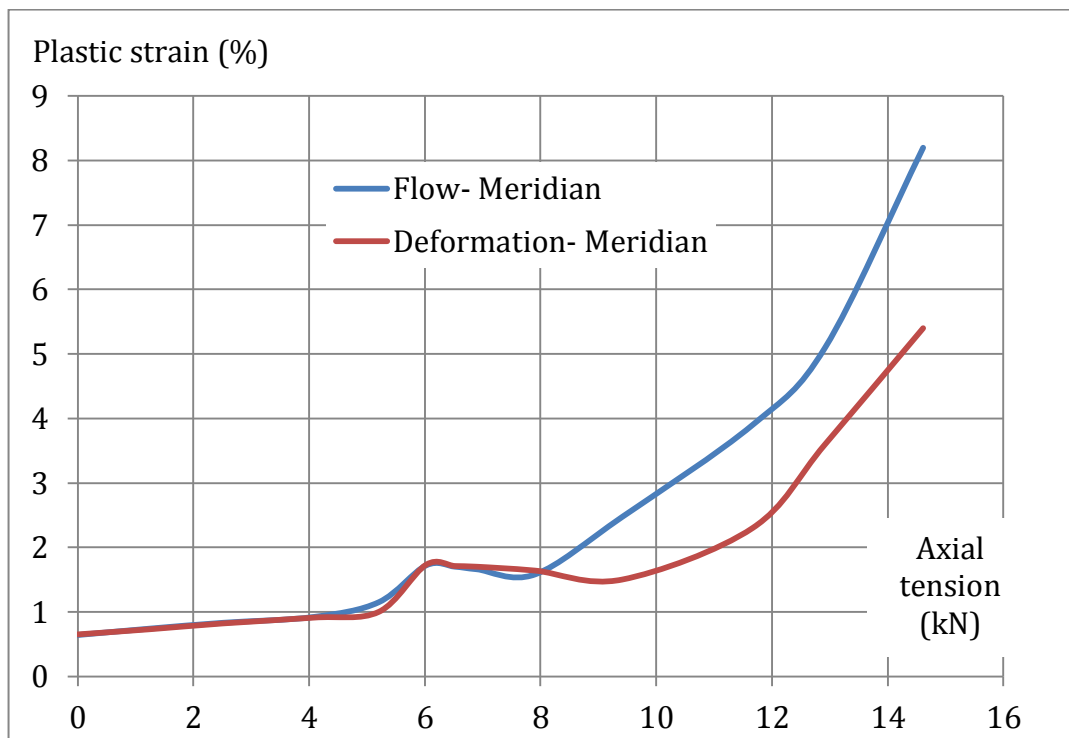
Figure 4.6: Maximum meridian plastic strains (Set A).
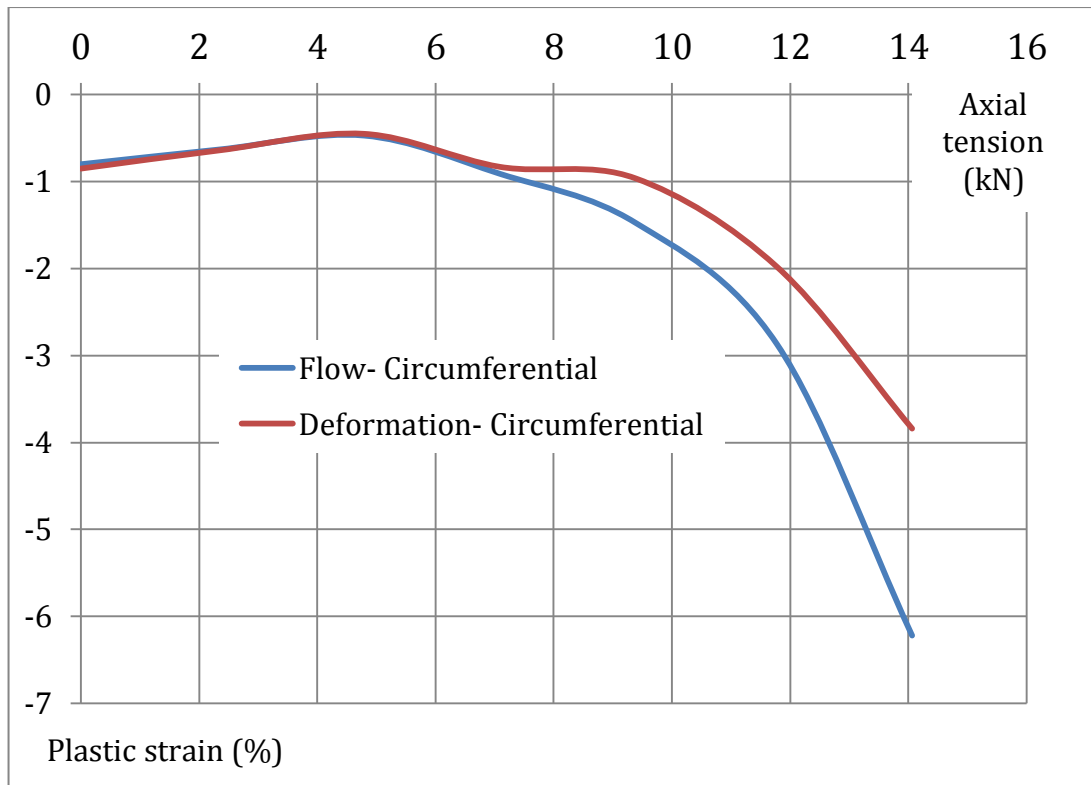
Figure 4.7: Maximum circumferential plastic strains (Set B).
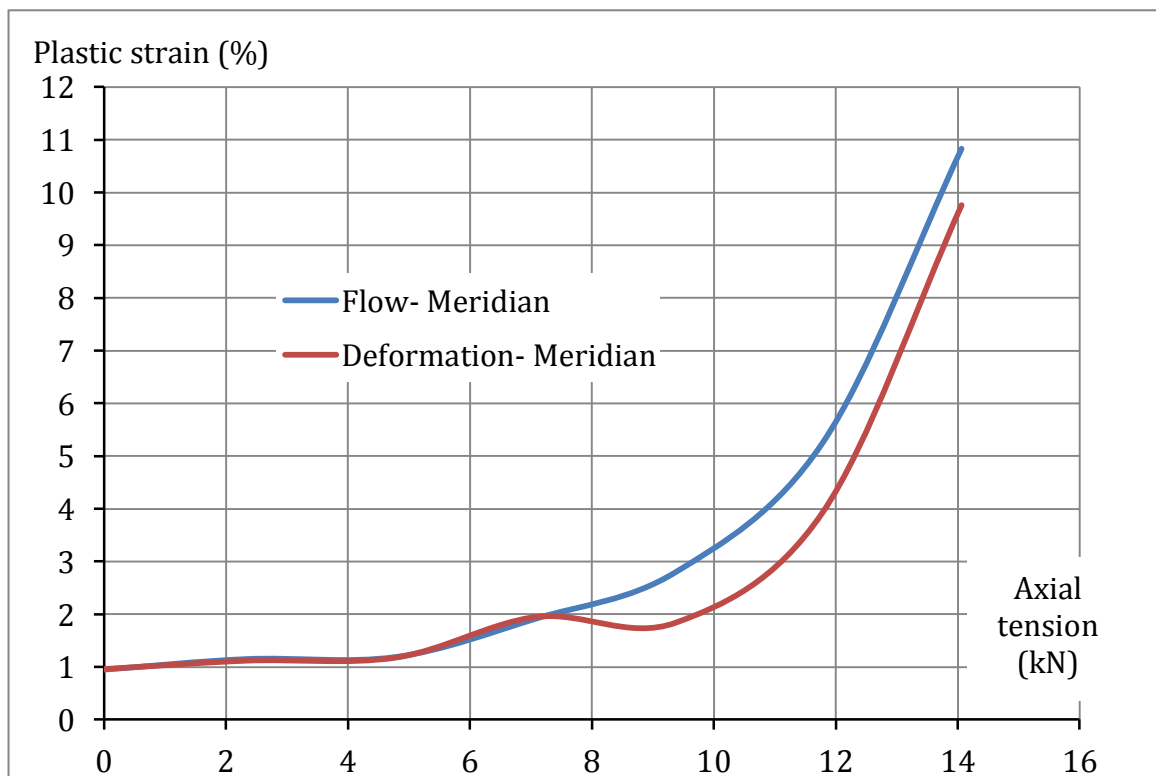
Figure 4.8: Maximum meridian plastic strains (Set B).

5. Imperfection sensitivity analysis

All the presented plastic buckling pressures have been obtained by assuming imperfections based on the experimentally observed buckling modes. Since this might appear a key point in obtaining a very good agreement with experimental results, in this Section the influence of the choice of the eigenmode used to generate the imperfect initial shape will be investigated in depth. To this purpose the results of additional numerical analyses conducted for specimens SP.6-Set B and SP.10-Set A, studied by Giezen et al. (1991) are presented.

In a first set of analyses, reported in section 5.1, 3 separate cases are considered in which the initial imperfection, of varying size, is generated by three different eigenmodes. For the same specimens a second set of analyses, reported in Section 5.2, have also been conducted, in which the imperfection was generated as a linear combination of the same three eigenmodes considered in Sub-section 5.2.

Furthermore, in Section 5.3 the analyses for the same specimens were performed again using BOSOR5, combining a nonlinear analysis of the axialsymmetric perfect cylinder with an eigenvalue analysis based on harmonic variation of radial displacements in the circumferential direction.

5.1 Imperfections generated by different eigenmodes

The results reported in this section are relative to specimens SP.6-Set B and SP.10-Set A, which were studied by means of a non-linear analysis of the imperfect cylinders with imperfection sizes varying from 1% to 14% of the thickness, and the imperfection shapes based on the first, third and fifth elastic eigenmodes, which correspond to a number n of circumferential waves equal to five, four and six, as shown in Figure 5.1.

| n=5	n=4	n=6
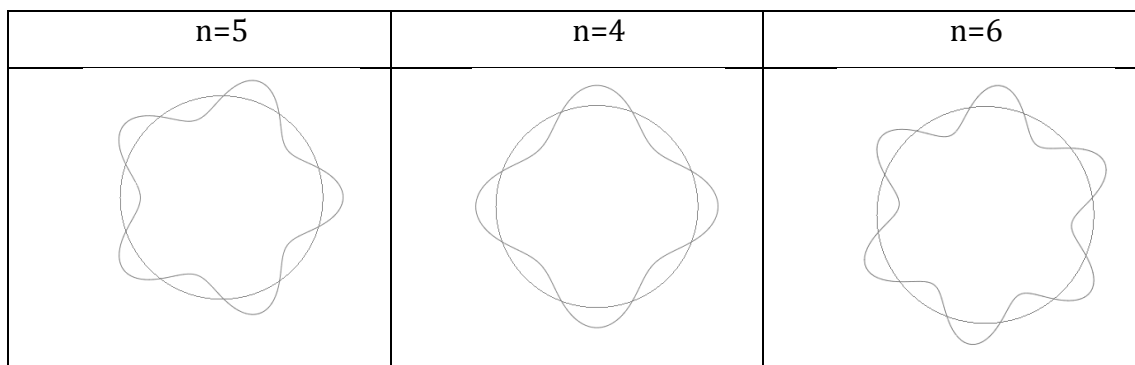
Figure 5.1: Imperfection distribution considered in this analysis

Figure 5.2 shows, as it was expectable, that the buckling pressures are sensitive to the size and shape of imperfection. The imperfection shape based on the linear elastic eigenmodes with 5 waves, which provides the lowest elastic buckling pressure, also provides the lowest plastic buckling pressure. Moreover, the buckling pressure values predicted by the deformation theory are lower than those predicted by the flow theory. The discrepancies between the flow and deformation theories results vary from 18.7% to 8.5% for the case of SP.6-Set B and from 8% to 2% for the case of SP.10-Set A. It can be also noticed that the discrepancies between both plasticity theories decrease with increasing imperfection ratios.
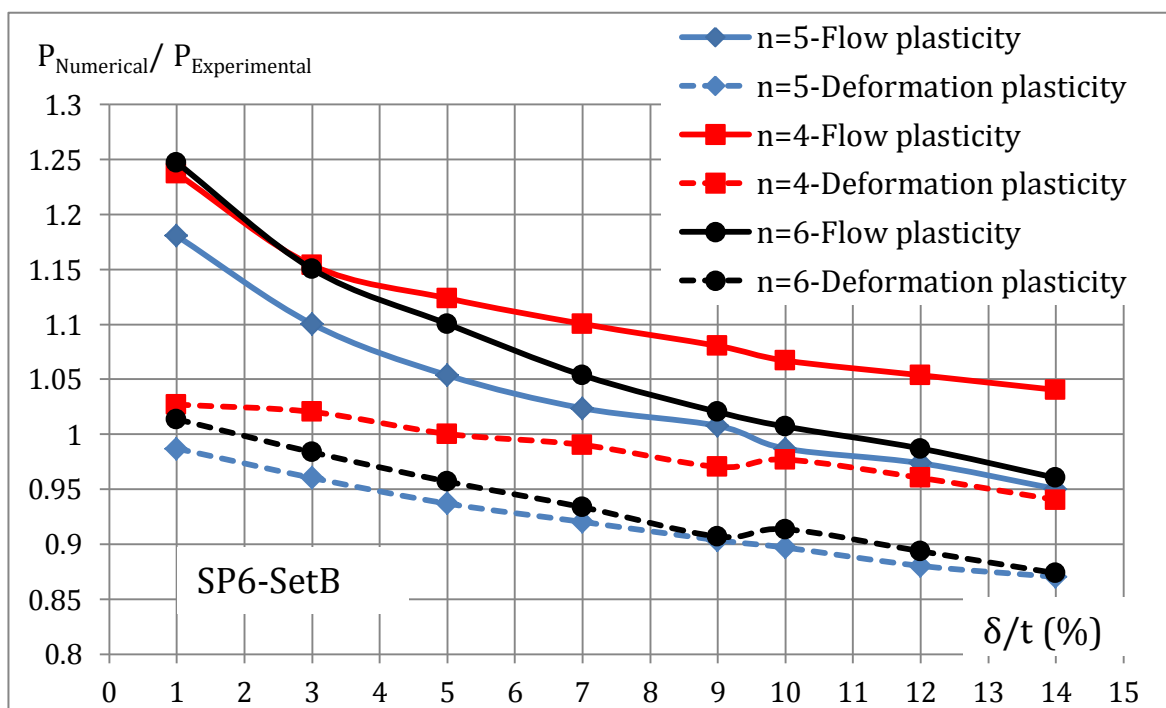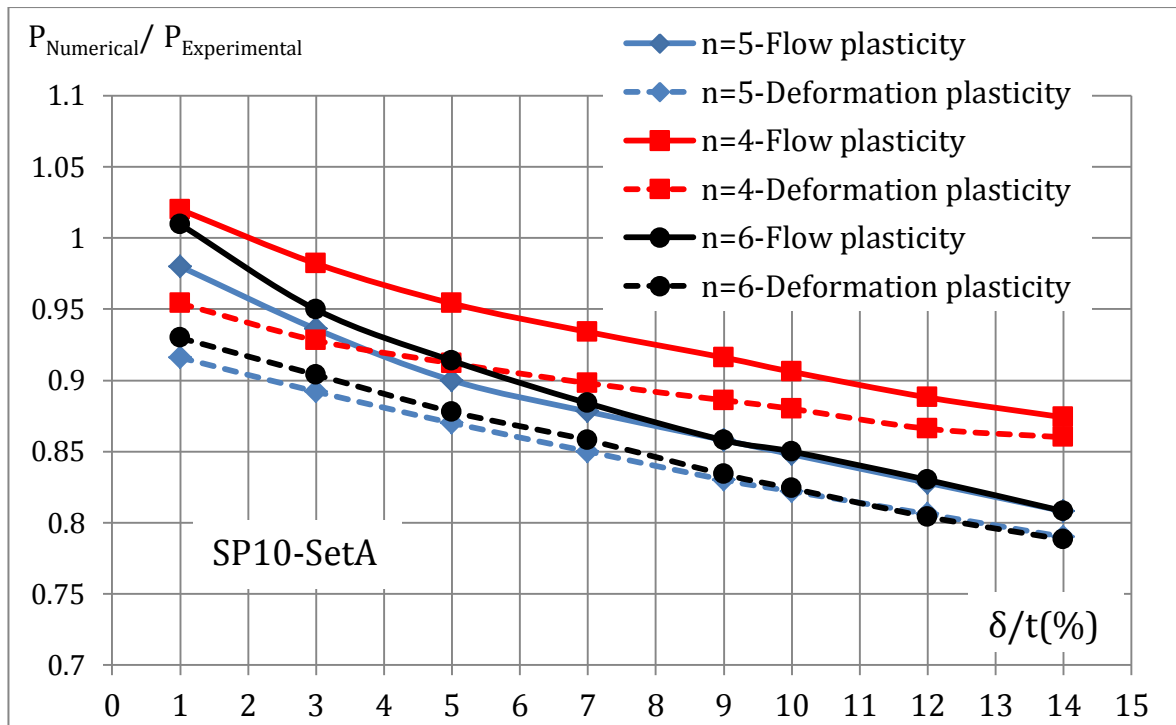
Figure 5.2: Effect of imperfections size and shapes on the buckling pressure calculated using the flow and deformation theories of plasticity.

5.2 Imperfections generated by a linear combination of different eigenmodes

The nonlinear analyses reported in this section, again with reference to specimens SP.6-Set B and SP.10-Set A, were based on imperfections generated from a linear combination of the same three eigenmodes considered in section 5.1. The largest contribution within the linear combination was assigned to the fifth eigenmode, because four waves were observed experimentally at failure.

Tables 5.1 and 5.2 show that both the flow and the deformation theory provide results that are in overall good agreement with the test results and that the deformation theory provides buckling pressures slightly lower than the flow theory. For both theories, the results are influenced by all the modes considered in the combination. For example, the addition of 2% of the 5- and 6-wave mode to a 3% 4-wave mode results in a change of the buckling pressure from 1.15 MPa to 1.09 MPa. The fact that all the considered eigenshapes contribute to the failure mode can be seen in Table 5.3 where, for two cases, the undeformed and deformed shape at the middle cross section of the cylinder is shown, before and after buckling and using both theories. This result is in

good agreement with the experimental finding reported by Giezen (1988), for instance in Figures 3.13 and 3.21 of his work, where the radial displacements present a rather irregular profile, which cannot be easily identified with a particular one of the eigenmode shapes.

	N. of waves	Imperfection amplitude (% of shell's thickness)	$P_{Flow} / P_{Experimental}$	$P_{Deformation} / P_{Experimental}$
Case 1	4	2	1.14	0.98
	5	1		
	6	1		
Case 2	4	3	1.09	0.96
	5	2		
	6	2		
Case 3	4	6	1.06	0.94
	5	2		
	6	2		
Case 4	4	10	1.04	0.93
	5	2		
	6	2		
Case 5	4	10	0.97	0.89
	5	5		
	6	5		
Case 6	4	10	0.9	0.83
	5	10		
	6	10		

Table 5.1: Buckling pressures for specimen SP.6-Set B obtained from our numerical analysis (ABAQUS) based on the flow and deformation theories. 4, 5 and 6 waves are used to seed the imperfection (P is the plastic buckling pressure).

	N. of waves	Imperfection amplitude (% of shell's thickness)	P_{Flow} / $P_{Experimental}$	$P_{Deformation}$ / $P_{Experimental}$
	4	2		
Case 1	5	1	0.96	0.91
	6	1		
	4	3		
Case 2	5	2	0.92	0.87
	6	2		
	4	6		
Case 3	5	2	0.91	0.86
	6	2		
	4	10		
Case 4	5	2	0.88	0.86
	6	2		
	4	10		
Case 5	5	5	0.83	0.82
	6	5		
	4	10		
Case 6	5	10	0.77	0.77
	6	10		

Table 5.2: Buckling pressures for specimen SP.10-Set A obtained from our numerical analysis (ABAQUS) based on the flow and deformation theories and using a combination of imperfections generated with 4, 5 and 6 waves.
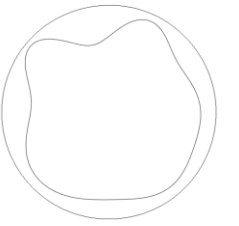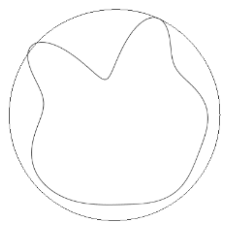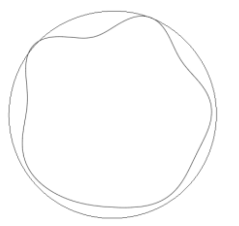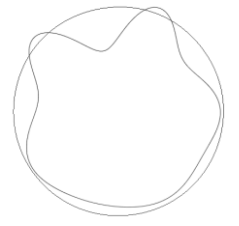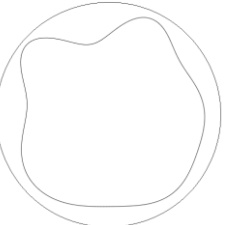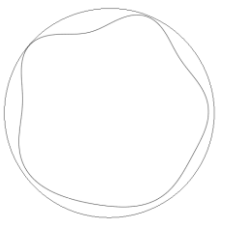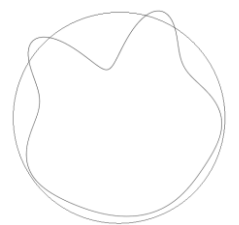
	Flow theory		Deformation theory	
	Buckling pressure	After buckling pressure	Buckling pressure	After Buckling pressure
Case1				
Case2				

Table 5.3: The deformed shape at the mid-section of the SP.6-Set B cylinder at the buckling pressure and after buckling pressure (the deformation is 10 times enlarged and the outer circle of each picture represents the un-deformed shape of the cylinder).

5.3 Bifurcation analysis for a perfect model using BOSOR 5 and an asymptotic approach in ABAQUS

While the results of the nonlinear analyses conducted using the flow theory in ABAQUS are in good agreement with the test results, similar analyses conducted in BOSOR5 tend to strongly over-predict plastic buckling pressures, by about 100% and 29% for SP.6-Set B and SP.1-Set A cylinders, respectively, as reported in Table 5.4. The procedure used in BOSOR5 is discussed in detail in Section 6.1, but here it is worth noticing that no imperfection are introduced and that bifurcations are searched by means of an eigenvalue analysis using a tangent stiffness matrix that accounts for the elasto-plastic material stiffness and is computed assuming a harmonic variation of the radial displacement with a predefined number n of circumferential waves.

Specimen	P_{Exp} (MPa)	Flow theory-BOSOR5			Deformation theory-BOSOR5		
		P(MPa)	$P/P_{Exp.}$	Number of waves	P(MPa)	$P/P_{Exp.}$	Number of waves
SP.6-Set B	2.99	6.12	2.04	3	3.20	1.1	5
SP.10-Set A	5.02	6.5	1.29	4	4.83	0.97	5
S5	8.25	NB	NB	NB	8.71	1.05	5

Table 5.4: Buckling pressures and corresponding buckling modes obtained from BOSOR5 code based on the flow and deformation theories.

In ABAQUS it is not possible to compute the bifurcation loads with a similar procedure, that is using a geometrically perfect model in the elastoplastic range. This is because, even if an eigenvalue buckling analysis can be conducted starting from a "base state geometry" equal to "the deformed geometry at the end of the last general analysis step, … during an eigenvalue buckling analysis, the model's response is defined by its linear elastic stiffness in the base state. All nonlinear and/or inelastic material properties, as well as effects involving time or strain rate, are ignored" (Simulia, 2011).

Therefore, in order to estimate the bifurcation load for a perfect model, an asymptotic procedure was used in ABAQUS for the two specimens S5 and SP.6-Set B, using six different values for imperfection amplitudes. The values of the imperfection amplitudes were 0%-0.05%-0.1%-1%-10% -50%. Four circumferential waves were chosen to generate the initial imperfection as this was the number waves observed

experimentally. Figures 5.3 and 5.4 show the equilibrium curves of the external pressure versus the radial displacement. It can be appreciated that, with a progressively decreasing amount of imperfection, the load-displacement curve tends towards a limit curve, which however does not coincide with the curve obtained for a perfect cylinder. The point where these deviate is the bifurcation point for the perfect model.
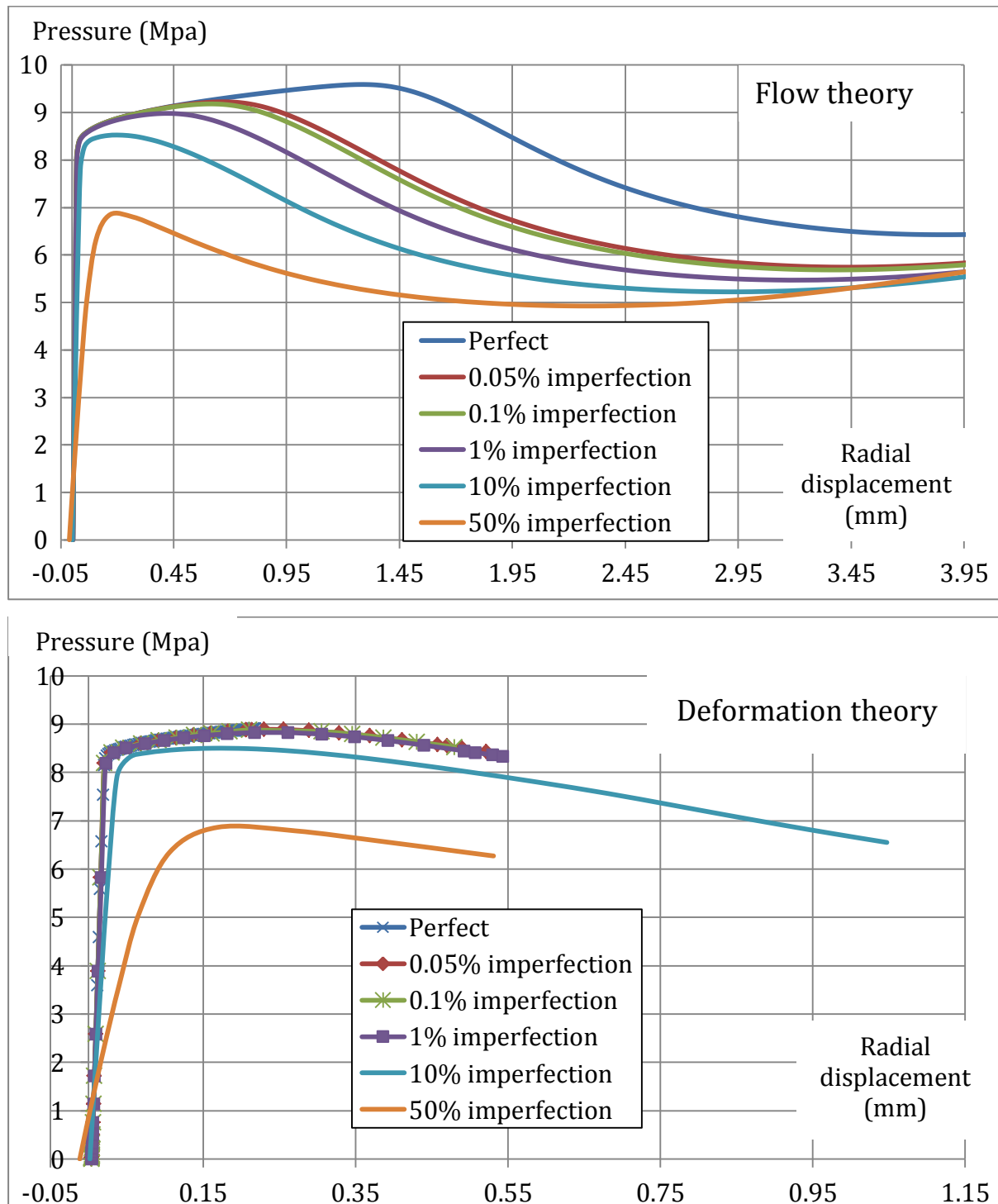

Figure 5.3: External pressure vs. radial displacement curves for specimens S5 (upper value of the yield stress) for different imperfection amplitudes
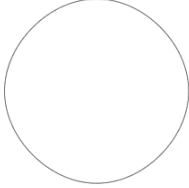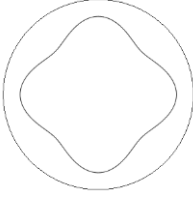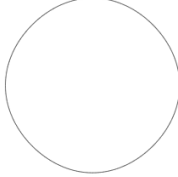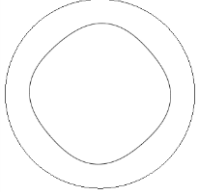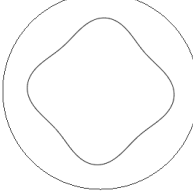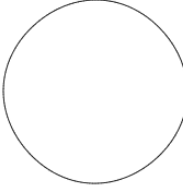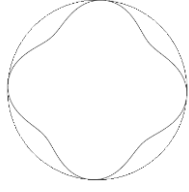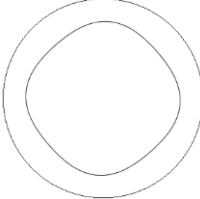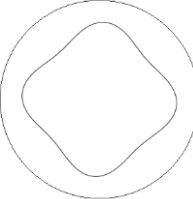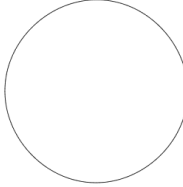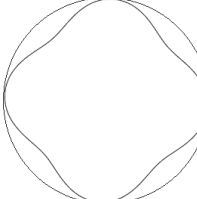
	Flow theory		Deformation theory	
	At the onset of buckling pressure	Post buckling path	At the onset of buckling pressure	Post buckling path
Perfect				-------
0.05% imperfection				
0.1% imperfection				

Table 5.5: The deformed shape at the mid-section of the S5 cylinder at the buckling pressure and after buckling pressure (Deformation is 10 times enlarged)

The buckling pressure for the cylinder S5 calculated in the present numerical analysis using the flow theory with 0.05% imperfection is equal to 9.23MPa while the flow theory employed in BOSOR5 code fail to predict plastic buckling pressure, as shown in Table 5.3. Moreover, the buckling pressure of the cylinder SP.6-Set B calculated in the present numerical analysis using the flow theory with 0.05% imperfection is equal to 4.05MPa while the flow theory employed in BOSOR5 code over-predicts plastic buckling pressure.
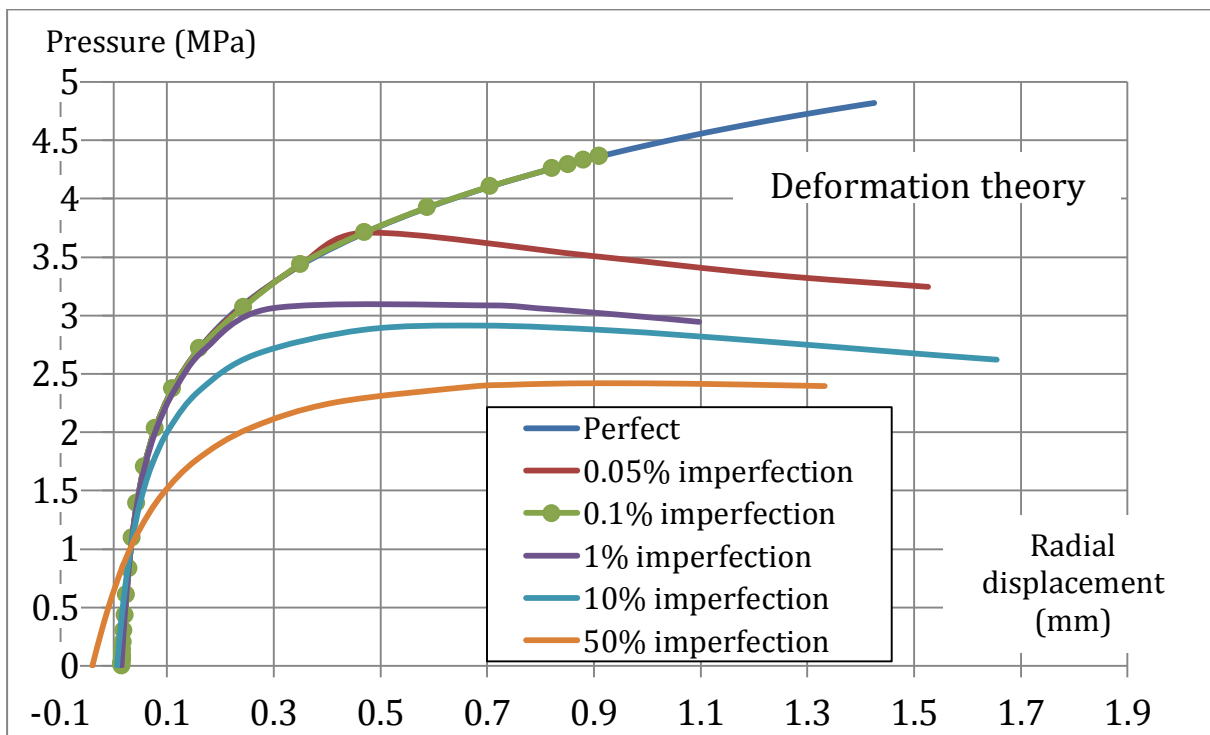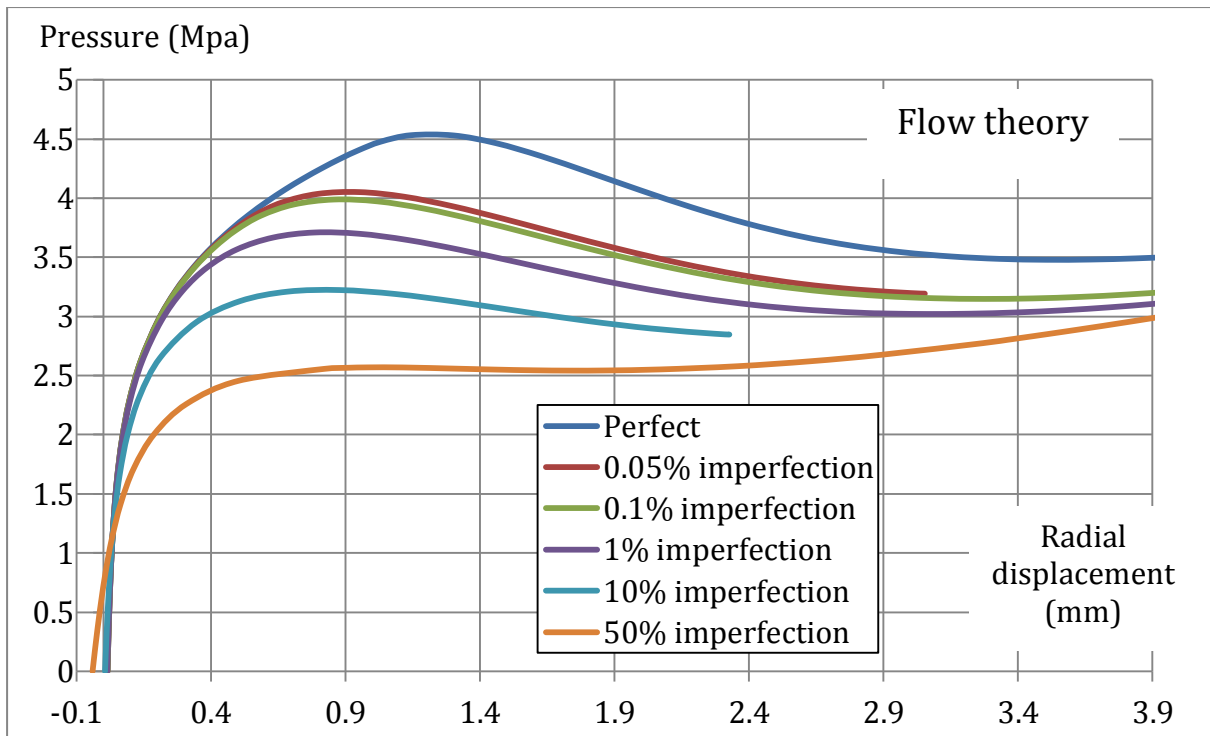
Figure 5.4: External pressure vs. radial displacement curves for specimens SP.6-Set B (upper value of the yield stress) for different imperfection amplitudes

Overall, the performed sensitivity imperfection analyses confirm the fact that, according to the present numerical studies, the flow and the deformation theory of plasticity tend to yield very similar results when the predominant imperfection coincides with the experimentally observed buckling mode. At the same time they show that for progressively different imperfection modes, the difference between the results from the flow and deformation theory tend to increase but significantly less than observed in other previous numerical treatments.

	Flow theory		Deformation theory	
	At the onset of buckling pressure	Post buckling path	At the onset of buckling pressure	Post buckling path
Perfect				------
0.05% imperfection				
0.1% imperfection				-------

Table 5.6: The deformed shape at the mid-section of the SP.6-Set B cylinder at the buckling pressure and after buckling pressure (Deformation is 10 times enlarged)

6. Discussion

6.1 A brief analysis of the procedure used in BOSOR5

It is worth noticing that the bifurcation load in the plastic range and the corresponding buckling mode for axisymmetrically loaded shells is determined in BOSOR5 through a sequence of two consecutive analyses (Bushnell, 1982). The first one is a nonlinear pre-buckling analysis which is valid for small strains and moderately

large rotations and accounts for material nonlinearity. This nonlinear problem is solved using a strategy in which nested iteration loop are applied at each load level. The inner loop is used to analyse the nonlinear behaviour caused by the moderately large displacements using the Newton-Raphson method. The outer loop is used to evaluate the constitutive matrix and the plastic strain components, and to test loading and unloading condition in the material by means of a sub-incremental strategy (Bushnell, 1982). The results from this analysis are used in the following analysis, which is an eigenvalue analysis which yields the bifurcation load and the corresponding axisymmetric or non-symmetric buckling mode, respectively (Bushnell, 1982). At the bifurcation load the infinitesimal displacement field, has components in the axial, circumferential and radial direction denoted as $\delta u, \delta v$ and δw. They are assumed to vary harmonically around the circumference as follows (Bushnell, 1984)

$$
\begin{cases}
\delta u = u_m(s) \sin n\theta \\
\delta v = v_m(s) \cos n\theta \\
\delta w = w_m(s) \sin n\theta
\end{cases}
\tag{6.1}
$$

where n is the number of circumferential waves, s and θ are the arc length of the shell measured along the reference surface and the circumferential coordinate, respectively. BOSOR5 users are asked to specify the range of circumferential wave numbers (n_{min} and n_{max}), and the starting wave number, n_o, which might correspond, in the user's judgment, to the minimum bifurcation load. BOSOR5 calculates the determinant of the global stability stiffness matrix for the chosen n_o (K_{1n_o}) at each time increment until the determinant changes sign. If the determinant of the stiffness matrix changes sign, BOSOR5 sets up, for all the values of n ranged between n_{min} and n_{max}, a series of eigenvalue problems of the form illustrated in the equations (Bushnell, 1982)

$$
(K_{1n} + \lambda_n K_{2n})(q_n) = 0
\tag{6.2}
$$

where K_{1n} and K_{2n} are the stiffness matrix and load-geometric matrix corresponding to m circumferential waves, respectively, and λ_n and q_n are the eigenvalues and eigenvectors for the numbers of wave n, respectively. The critical wave number

n_{cr} corresponds to the minimum value of λ_n. The strategy used to identify buckling load is explained in detail in Bushnell (1982).

It is important to note that the discretisation in BOSOR5 is only performed in the meridian direction because the resulting displacements are axisymmetric in the pre-buckling phase and the buckling mode is assumed to vary harmonically in the circumferential direction in the bifurcation buckling analysis (Bushnell, 1982).

6.2 Interpretation of the presented FE results in the context of the plastic buckling paradox

The main findings from the numerical results presented in Sections 3, 4 and 5 are the following:

(i) When an accurate and consistent FE model is set up, both the flow and deformation theories can predict buckling loads within acceptable plastic strains for different values of applied axial tensile load;

(ii) Buckling pressures calculated numerically by means of the flow theory are generally in better agreement with the experimental data.

These results are in contrast with the conclusions obtained by Blachut et al. (1996) and Giezen et al. (1991) by means of the code BOSOR5. In fact, according to BOSOR5 the flow theory tends to overpredict the values of the buckling pressure and of the plastic strains while the deformation theory results are more in line with the experimental results.

In general, it has been observed BOSOR5 is not a very good predictor of non-axisymmetric buckling because it does not handle pre-buckling transverse shear deformation and non-axisymmetric initial imperfections (Bushnell, private communication). In fact, for a long time it was believed that the difference in buckling predictions between flow versus deformation theory was entirely caused by the difference in the effective shear modulus used for the bifurcation buckling phase of the analysis (Onat and Drucker, 1953). However, Giezen (1988) showed, using the code BOSOR5, that in the case of cylinders under non-proportional loading the adoption of the effective shear modulus predicted by the deformation theory, $\overline{G}$, instead of the

elastic one, G, in the flow theory does lead to a certain reduction in the value of the buckling load but not as much as to make it comparable with the predictions from the deformation theory, based on the secant modulus in shear.

Table 5.4 clearly shows that, although this modification is used in the BOSOR5 calculations based on the flow theory of plasticity (Bushnell, 1974), the results still overestimate the experimental buckling pressures or even fail to predict buckling at all. It is so clear that the difference in buckling predictions between flow versus deformation theory can be only partially attributed to the difference in the effective shear modulus used for the bifurcation buckling phase of the analysis.

The discrepancies between the numerical results from the presented study, particularly in terms of buckling pressure, and those obtained numerically using BOSOR5 can be explained by analysing the type of assumptions made in BOSOR5.

In fact, Shamass et al. (2014) already concluded, in the case of proportional loading, that the simplifying assumptions on the buckling shape made in several analytical treatments, which result in a sort of kinematic constraint, lead to an excessive stiffness of the cylinders and, consequently, to an overestimation of the buckling stress for both the flow and deformation theories. However, the deformation theory tends to compensate this kinematic overstiffness and provides results that are more in line with the experimental ones.

This fact seem confirmed also in the case of non-proportional loading by the presented comparison between the FE results and those obtained by Blachut et al. (1996) and Giezen et al. (1991) using BOSOR5. In fact, BOSOR5 assumes that the buckling shapes vary harmonically in the circumferential direction. Once again, this assumption regarding the kinematics of the problem seems to be the main reason for the systematic discrepancies between the results from BOSOR5 based on the flow theory of plasticity and those from the numerical analyses performed in the present study, especially when a noticeable value of axial loading is applied.

7. Conclusions

The present study has been addressed to a further understanding of the apparent discrepancy between the predictions of the flow and the deformation theory of plasticity on the basis of accurately modelled and conducted FE analyses of cylinders

under non-proportional loading. By comparing the obtained results with some experimental and numerical results in literature, it has been found that the FE predictions based on the flow theory of plasticity result in good agreement with the experimental findings. This is in contrast with the conclusions by other authors, who reported that the results from the flow theory led to incorrect predictions of plastic strains and buckling pressures and that the deformation theory led to much more accurate predictions.

The root of the discrepancy can be thought to lay, once again (see Shamass et al., 2014, 2015), in the harmonic buckling shapes assumed in the circumferential direction. This fact leads to overestimate the buckling pressures when the flow theory of plasticity is employed, while the deformation theory tends to counterbalance the excessive kinematic stiffness and apparently provides results which are more in line with the experimental findings.

Also in the case of cylinders subjected to non-proportional loading it can thus be concluded that there does not seem to be any plastic buckling paradox.

Acknowledgements

References

Ambartsumjan, S.A. On the stability of inelastic plates with consideration of shear deformation. PMM: Prikladnaya Matematika I Mekhanika (in Russian) 1963;27:753-757.

Bardi, F.C. and Kyriakides, S. Plastic buckling of circular tubes under axial compression - Part I: Experiments. Int J Mech Sci 2006;48:830-841.

Batdorf, S.B and Budiansky, B. A mathematical theory of plasticity based on the concept of slip, NACA Tech Note 1949;1871:1-36.

Blachut, J., Galletly, G.D and James, S. On the plastic buckling paradox for cylindrical shells. Proceedings of the Institution of Mechanical Engineers, Part C J Mech Eng Sci 1996; 210:477-488.

Blachut, J. and Galletly, G. D. Influence of local imperfections on the collapse strength of domed end closures. Proceedings of the Institution of Mechanical Engineers, Part C J Mech Eng Sci, 1993; 207:197-207.

Bushnell, D. BOSOR5 – Program for buckling of complex, branched shells of revolution including large deflections, plasticity and creep. In Structural Analysis Systems – Vol. 2, edited by Niku-Lari, A. Pergamon 1986;25-54.

Bushnell, D. Computerized analysis of shells-governing equations. Comput Struct 1984; 18:471 - 536.

Bushnell, D. Plastic buckling, in pressure vessels and piping: Design Technology – 1982, A Decade of Progress, edited by Zamrik, S. Y. and Dietrich, D. ASME 1982:47-117.

Bushnell, D. Bifurcation buckling of shells of revolution including large deflections, plasticity and creep. Int J Solids Struct 1974;10:1287-1305.

Bushnell, D. Private communication. 2015

Falzon, B.G. An introduction to modelling buckling and collapse. Glasgow, UK, NAFEMS Ltd;2006

Giezen, J.J, Babcock, C. D. and Singer, J. Plastic buckling of cylindrical shells under biaxial loading. Exp Mech 1991;31:337-343

Giezen, J.J. Plastic buckling of cylinders under biaxial loading. Ph.D thesis. California Institute of Technology, Pasadena, CA, February 1988.

Jahed H, Lambert S.B. and Dubey R.N. Total deformation theory for non-proportional loading. Int J Pres Ves Pip 1998;75:633–642.

Lay, M.G. Flange local buckling in wide-flange shapes. J Struct Div - ASCE 1965;91:95-116.

Mao, R. and Lu, G. Plastic buckling of circular cylindrical shells under combined in-plane loads. Int J Solids Struct 1999;38:741-757.

Onat, E. T. and Drucker, D. C. Inelastic instability and incremental theories of plasticity. AIAA 1953,20:181-186.

Ore, E. and Durban, D. Elastoplastic buckling of axially compressed circular cylindrical shells. IJMS 1992;34:727-742.

Peek, R. An incrementally continuous deformation theory of plasticity with unloading. Int J Solids Struct 2000;37:5009–5032.

Riks, E. An incremental approach to the solution of snapping and buckling problems. Int J Solids Struct 1979;15:529-551.

Shamass, R., Alfano, G. and Guarracino, F. A numerical investigation into the plastic buckling paradox for circular cylindrical shells under axial compression. Eng Struct J 2014;75:429-447.

Shamass, R., Alfano, G. and Guarracino, F. An analytical insight into the buckling paradox for circular cylindrical shells under axial and lateral loading. Math. Probl. Eng. 2015;ID 514267:1-11.

Sewell, M. J. A yield-surface corner lowers the buckling stress of an elastic-plastic plate under compression. J Mech Phys Solids 1973;21:19-45.

Simo J.C. and Hughes T.J.R. Computational inelasticity. Springer; 1998.

Simulia . ABAQUS User manual. Version 6.11-1.Dassault Systems; 2011.

Tuğcu, P. On plastic buckling predictions. Int J Mech Sci 1991;33:529-539.